Table 3. Pharmacokinetic parameters of temozolomide and MTIC plasma concentrations in cycle 1 (150 mg/m^2 per day) and cycle 2 (200 mg/m^2 per day)

Analyte	Dose (mg/m^2)	Dosing day	Tmax (h)	Cmax (μg/ml)	$t_{1/2}\lambda z$ (h)	AUC (μg·h/ml)			CL/F (ml/min per kg)	Vz/F (l/kg)	R	
						0–t	0–24	0–∞			Cmax	AUC_{0-24}
Temozolomide	150 (n = 6)	Day 1	1.42 (52)	7.87 (38)	2.14 (25)	25.7 (15)	26.5 (14)	26.1 (14)	2.57 (18)	0.468 (23)	–	–
		Day 5	0.958 (53)	8.38 (36)	2.29 (35)	25.2 (10)	25.9 (9)	25.6 (10)	2.56 (14)	0.492 (21)	1.11 (24)	0.986 (8)
	200 (n = 3)	Day 1	0.583 (25)	15.3 (5)	2.03 (4)	35.1 (6)	36.4 (6)	35.7 (6)	2.37 (5)	0.415 (7)	–	–
		Day 5	0.917 (57)	14.0 (30)	2.02 (5)	36.0 (4)	37.3 (5)	36.7 (4)	2.27 (9)	0.395 (5)	0.868 (39)	1.03 (7)
MTIC	150 (n = 6)	Day 1	1.42 (52)	0.145 (38)	1.98 (24)	0.426 (15)	0.451 (14)	0.463 (14)	–	–	–	–
		Day 5	1.08 (43)	0.154 (28)	1.83 (12)	0.425 (12)	0.445 (13)	0.454 (13)	–	–	1.14 (29)	1.00 (16)
	200 (n = 3)	Day 1	0.750 (33)	0.272 (15)	1.93 (6)	0.594 (7)	0.622 (8)	0.632 (8)	–	–	–	–
		Day 5	0.917 (57)	0.284 (33)	1.87 (3)	0.636 (7)	0.665 (7)	0.676 (7)	–	–	1.03 (17)	1.07 (1)

Values are means, with coefficient of variation % in parentheses
Tmax, time of each plasma concentration; Cmax, maximun plasma concentration; $t_{1/2}\lambda z$, elimination half-life terminal excretion phase; AUC, area under the plasma concentration time curve; CL/F, apparent total body clearance; Vz/F, apparent distribution volume; R, accumulation index

of the TMZ plasma concentrations on day 1 as well as on day 5. The tmax and $t_{1/2}\lambda z$ values of MTIC plasma concentrations were 0.750 to 1.42 h and 1.83 to 1.98 h, respectively, which closely matched the tmax and $t_{1/2}\lambda z$ values of the TMZ plasma concentrations. After the administration of 150 and 200 mg/m^2 per day, the Cmax values were 0.145 to 0.154 and 0.272 to 0.284 μg/ml, respectively; AUC_{0-t} values were 0.425 to 0.426 and 0.594 to 0.636 μg·h/ml, respectively; AUC_{0-24} values were 0.445 to 0.451 and 0.622 to 0.665 μg·h/ml, respectively; and $AUC_{0-\infty}$ values were 0.454 to 0.463 and 0.632 to 0.676 μg·h/ml, respectively. Cmax and AUC exhibited a dose-dependent increase in relation to the administration of 150 mg/m^2 per day and 200 mg/m^2 per day. The ratios of MTIC to TMZ, based on Cmax and AUC, were 1.78% to 2.03% and 1.66% to 1.84%, respectively. The accumulation index, based on Cmax and AUC_{0-24}, was 1.03 to 1.14 and 1.00 to 1.07, indicating no accumulation due to repeated administration, as in the case of TMZ plasma concentrations. The coefficients of variation for AUC and $t_{1/2}\lambda z$ ranged from 3% to 24%.

TMZ urinary excretion rate

Table 4 shows the amount of urinary excretion, excretion rate, and renal clearance by urine accumulation intervals to 24 h after the administration of TMZ on days 1 and 5 in the first cycle (150 mg/m^2 per day) and second cycle (200 mg/m^2 per day). One of the three patients in the second cycle mistakenly discarded the 0- to 4-h urine after administration on day 5, and the cumulative urinary excretion data for this patient on day 5 of the administration of 200 mg/m^2 per day was considered missing.

The cumulative urinary excretion rates of TMZ (up to 24 h after administration) were 7.42% and 5.93% on days 1 and 5, respectively, at 150 mg/m^2 per day, and 4.81% and 5.21% on days 1 and 5, respectively, at 200 mg/m^2 per day. The renal clearance of TMZ was 0.193 and 0.155 ml/min per kg on days 1 and 5, respectively, at 150 mg/m^2 per day, and 0.114 and 0.119 ml/min per kg on days 1 and 5, respectively, at 200 mg/m^2 per day. No change due to the difference in dose or to repeated administration was observed in the urinary excretion rate or renal clearance of TMZ. Calculation of the proportion of renal clearance to total body clearance (2.27–2.57 ml/min per kg) indicated a value of 4.81% to 7.51%.

Safety

Adverse events occurred in all patients; most of these events were either mild or moderate.

The adverse events observed at an incidence of 50% or more were: constipation in 67% (four patients), nausea in 67% (four patients), increased alanine aminotransferase in 67% (four patients), increased aspartate aminotransferase in 67% (four patients), and increased blood alkaline phosphatase in 50% (three patients). These adverse events also corresponded to the adverse events for which a causal rela-

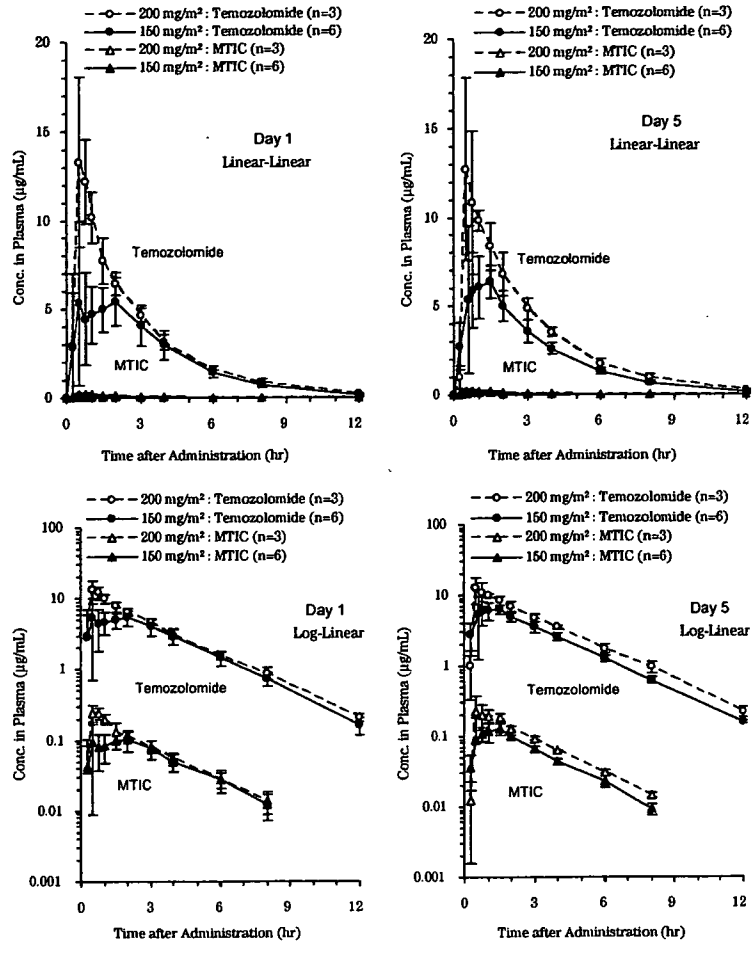

Fig. 1. Time-course change in mean plasma temozolomide and 5-(3-methyl)1-triazen-1-yl-imidazole-4-carboxamide (*MTIC*) concentrations on days 1 and 5 in cycle 1 (150 mg/m^2 per day) and cycle 2 (200 mg/m^2 per day)

Table 4. Amount of urinary temozolomide excretion (Ae), excretion rate (Ae%), and renal clearance (CLr) by urine accumulation intervals in cycle 1 (150 mg/m^2 per day) and cycle 2 (200 mg/m^2 per day)

Parameter	Dose (mg/m^2)	Administration day	Time after administration (Urine accumulation interval) (h)			
			0–4	4–8	8–24	0–24
Ae (mg)	150	Day 1	11.1 (25)	5.64 (59)	1.49 (82)	18.2 (22)
	$n = 6$	Day 5	10.3 (43)	3.37 (46)	0.915 (55)	14.6 (26)
	200	Day 1	12.8 (53)	3.42 (62)	0.178 (173)	16.4 (53)
	$n = 3$	Day 5	12.8[a]	3.93 (32)	1.00 (89)	17.7[a]
Ae% (%)	150	Day 1	4.51 (29)	2.32 (65)	0.593 (80)	7.42 (28)
	$n = 6$	Day 5	4.20 (48)	1.36 (47)	0.366 (55)	5.93 (33)
	200	Day 1	3.75 (57)	1.00 (66)	0.0524 (173)	4.81 (57)
	$n = 3$	Day 5	3.75[a]	1.15 (36)	0.300 (90)	5.21[a]
CLr (ml/min per kg)	150	Day 1	–	–	–	0.193 (33)
	$n = 6$	Day 5	–	–	–	0.155 (42)
	200	Day 1	–	–	–	0.114 (60)
	$n = 3$	Day 5	–	–	–	0.119[a]

Values are means, with coefficient of variation % in parentheses
[a] $n = 2$

tion to TMZ could not be ruled out (adverse reactions) that were observed at an incidence of 50% or more.

As myelosuppression-related adverse events, a decrease in neutrophil count (grade 2), platelet count (grade 1), and leukocyte count (grade 2) occurred in one patient each (17%). Grade 3 toxicity observed in hematology tests was a decreased lymphocyte count in one patient, and no other grade 3 or 4 toxicity was observed. Leukocyte count, platelet count, and neutrophil count were within normal ranges. No grade 3 or 4 toxicities were observed in biochemistry tests or urinalysis, except for a grade 3 increase in alanine aminotransferase in two patients.

Two adverse events resulted in death. The first was brain damage in one patient, resulting in death 23 days after the final administration in the first cycle. The second was a decreased level of consciousness in one patient who discontinued participation in the study 23 days after the final administration in the first cycle and who died about 3 months after discontinuation. The study was also discontinued in another patient 24 days after the final administration in the sixth cycle due to progression of the primary disease, and this patient died about 3.5 months after discontinuation due to aggravation of the primary disease. Three deaths occurred in this study, but the cause of death in all three patients was attributed to the primary disease.

Discussion

We investigated the pharmacokinetics of TMZ in Japanese patients to determine whether or not the treatment regimen used in the United States and Europe could be used in Japan.

After the oral administration of 150 and 200 mg/m^2 per day, TMZ plasma concentration reached tmax about 1 h after administration, followed by a monophasic decrease. Although a dose-dependent increase in Cmax and AUC was observed, these values did not increase after 5 days of repeated administration (accumulation index was about 1), indicating no accumulation of this drug. The elimination of TMZ from plasma was rapid, and no change due to difference in the dose or to repeated administration was observed in CL/F or Vz/F. The coefficients of variation for AUC, $t_{1/2}\lambda z$, CL/F, and Vz/F were small, at 4% to 35%, suggesting that the interpatient difference in pharmacokinetics was small. Plasma MTIC concentrations were observed to change in parallel with TMZ plasma concentrations at both 150 and 200 mg/m^2 per day, and tmax and $t_{1/2}\lambda z$ values generally corresponded to those of TMZ plasma concentrations. The Cmax and AUC of MTIC plasma concentration were 1.8% to 2.0% and 1.7% to 1.8% of those of TMZ plasma concentrations. With TMZ, no accumulation was observed with repeated administration. These results suggested that the plasma MTIC concentration is dependent on the plasma TMZ concentration and that the reaction rate from MTIC to AIC is clearly more rapid than that from TMZ to MTIC. Based on the results obtained by the administration of 150 and 200 mg/m^2 per day, no marked change in pharmacokinetics due to the difference in dose or to repeated administration was noted. The cumulative urinary excretion rate of TMZ was 4.8% to 7.4% (up to 24 h after administration). The renal clearance of TMZ was 0.114 to 0.193 ml/min per kg, accounting for 4.8% to 7.5% of total body clearance. It is possible, however, that actual renal clearance was underestimated because of the possible effect of decomposition during the retention of urine in the bladder. The above plasma and urinary pharmacokinetic profile of TMZ in Japanese was essentially the same as that already observed in Caucasians.[8-10]

The pharmacokinetic parameters of TMZ and MTIC plasma concentrations in Japanese patients obtained in this study were compared with those obtained in pharmacokinetic studies (Schering-Plough data on file)[8,10,12] conducted

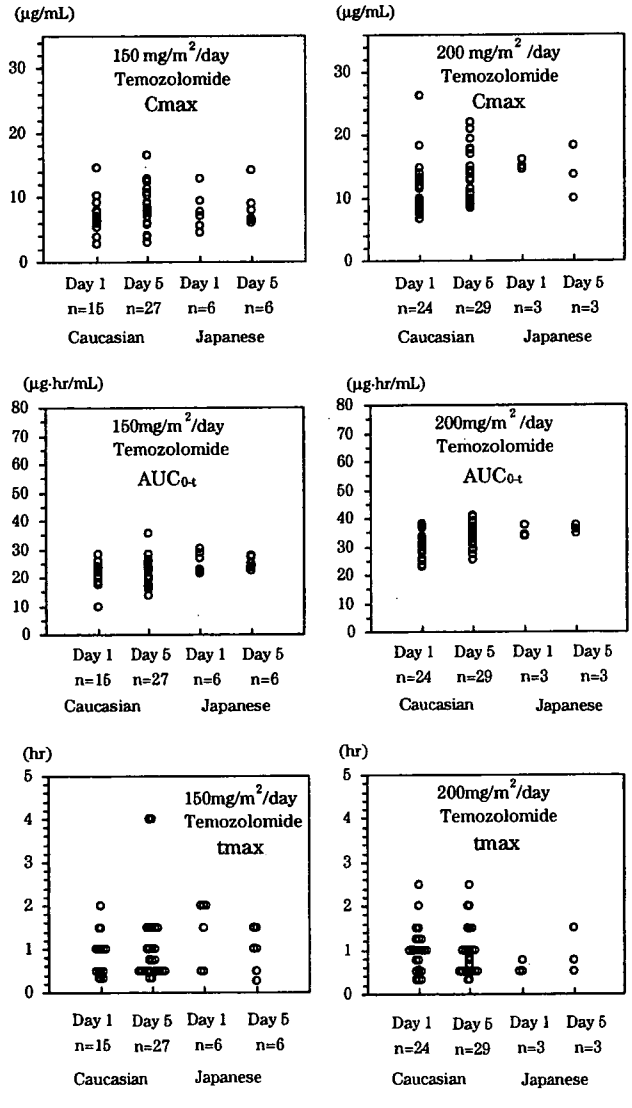

Fig. 2. Maximum plasma concentration (*Cmax*), area under the plasma concentration-time curve up to the final observation point ($AUC_{0\text{-}t}$), and time-to-maximum plasma concentration (*tmax*) of temozolomide: comparison between Japanese and Caucasians. Data of Caucasians are cited from Schering-Plough data on file[8,10,12]

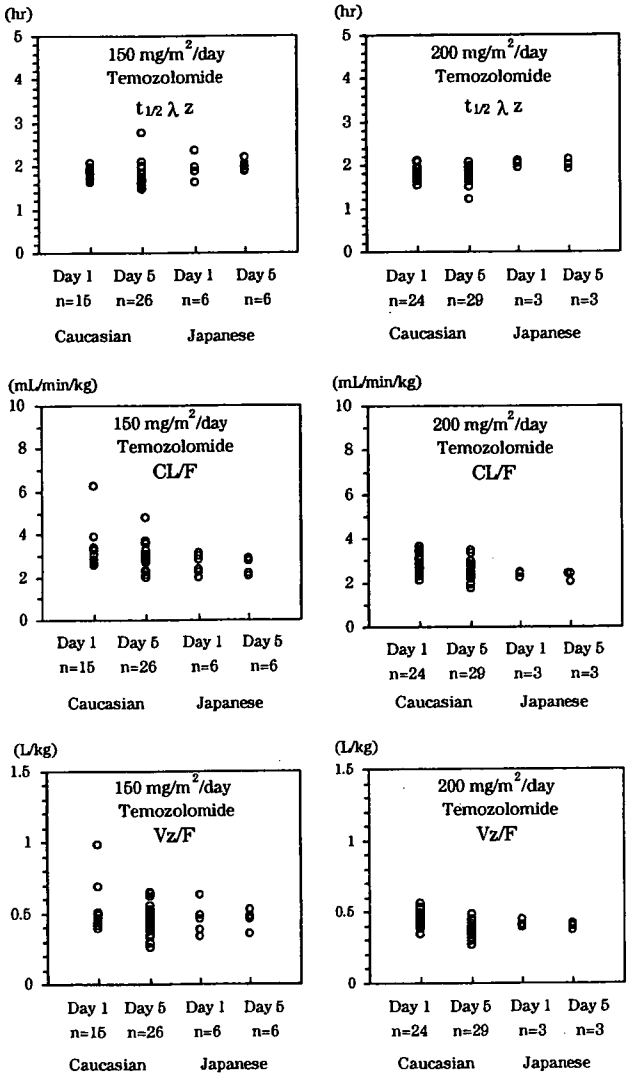

Fig. 3. Elimination half-life of terminal excretion phase ($t_{1/2}\lambda z$), apparent total body clearance (*CL/F*), and apparent distribution volume (*Vz/F*) of plasma temozolomide: comparison between Japanese and Caucasians. Data of Caucasians are cited from Schering-Plough data on file[8,10,12]

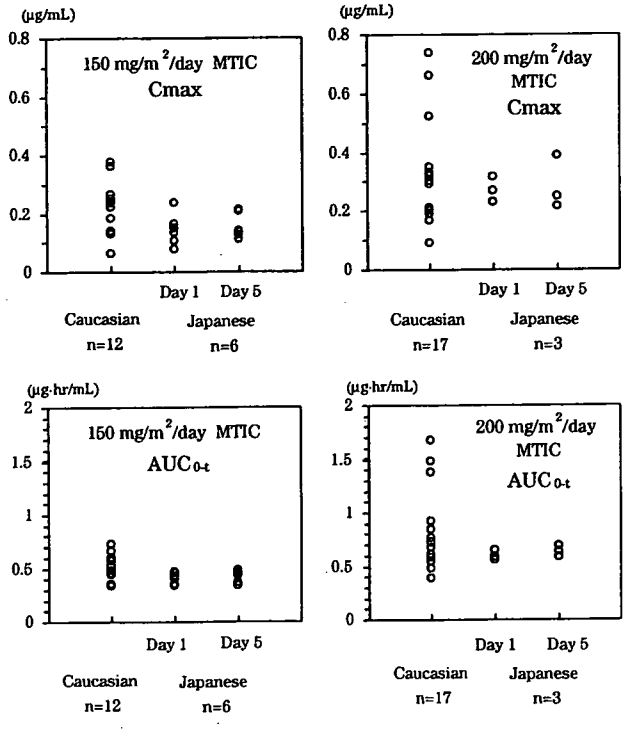

Fig. 4. Maximum plasma concentration (Cmax) and the area under the plasma concentration-time curve (AUC_{0-t}) of 5-(3-methyl)-1-triazen-1-yl-imidazole-4-carboxamide (MTIC) concentration: comparison between Japanese and Caucasians. Data of Caucasians are cited from Schering-Plough data on file[8,10,12]

in Caucasians in the United States. As shown in Figs. 2 to 5, the pharmacokinetic parameters (Cmax, tmax, AUC_{0-t}, $t_{1/2}\lambda z$, CL/F, and Vz/F) of plasma TMZ concentration and the pharmacokinetic parameters (Cmax, tmax, AUC_{0-t}, and $t_{1/2}\lambda z$) of plasma MTIC concentration obtained from Japanese patients all fell in the range of data obtained from Caucasian patients. These results confirm the assumption that there is little possibility that the pharmacokinetics of TMZ would be affected by biological factors including ethnic differences.

Adverse events occurred in all patients, but most were judged to be mild or moderate in severity. Continued administration was therefore possible with dose adjustment and delay in the start of administration of the next cycle. The incidence of nausea and constipation was high, but with prophylactic antiemetic administration during the administration period, no patient discontinued or interrupted treatment due to nausea during the 5 days of administration in each cycle. Constipation was managed with laxatives. Delay in the start of administration and dose modification due to myelosuppression was required in one of the four patients who continued to receive treatment with TMZ in the second cycle. The safe continuation of treatment was considered possible by monitoring for adverse reactions and adjusting the dose. No increase of myelosuppression with increased dose was observed.

The treatment regimen in this study was generally well tolerated in Japanese patients with relapsed gliomas.

The confirmation of the safety of TMZ in Japanese patients in this study contributes greatly to the assurance of safety in Asians, including patients in Taiwan and South Korea, where TMZ is already being used. The possibility is very high that the treatment regimen in the United States and Europe is applicable to all ethnic groups.

Conflict of interest

All authors declare no conflict of interest.

Acknowledgments This study was supported by Schering-Plough K.K. We are indebted to the patients and their families for agreeing to par-

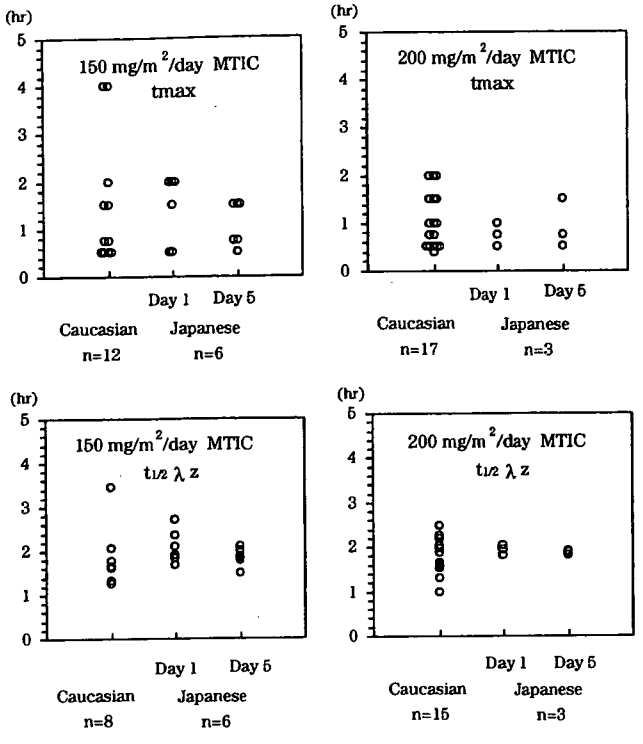

Fig. 5. Values for time of each plasma concentration (tmax) and terminal excretion phase ($t_{1/2}\lambda z$) of plasma 5-(3-methyl)-1-triazen-1-yl-imidazole-4-carboxamide (MTIC) concentration: comparison between Japanese and Caucasians. Data of Caucasians are cited from Schering-Plough data on file[8,10,12]

ticipate in this study, and to the study nurse and data managers for their collaboration.

References

1. Slack JA, Goddard C, Stevens MFG, et al. (1986) The analysis and murine pharmacokinetics of a new antitumor agent: CCRG 81045. J Pharm Pharmacol 38:63
2. Wheelhouse RT, Stevens MFG (1993) Decomposition of the antitumor drug temozolomide in deuteruated phosphate buffer: methyl group transfer is accompanied by deuterium exchange. J Chem Soc Chem Commun 15:1177–1178
3. Denny BJ, Wheelhouse RT, Stevens MFG, et al. (1994) NMR and molecular modeling investigation of the mechanism of activation of the antitumor drug temozolomide and its interaction with DNA. Biochemistry 33:9045–9051
4. Stevens MFG, Hickman JA, Langdon SP, et al. (1987) Antitumor activity and pharmacokinetics in mice of 8-carbamoyl-3-methyl-imidazo [5,1-d]-1,2,3,5-tetrazin-4(3H)-one (CCRG 81045: M&B 39831), a novel drug with potential as an alternative to dacarbazine. Cancer Res 47:5846–5852
5. Newlands ES, Stevenst MFG, Wedge SR, et al. (1997) Temozolomide: a review of its discovery, chemical properties, pre-clinical development and clinical trials. Cancer Treat Rev 23:35–61
6. Ostermann S, Csajka C, Buclin T, et al. (2004) Plasma and cerebrospinal fluid population pharmacokinetics of temozolomide in malignant glioma patients. Clin Cancer Res 10:3728–3736
7. Newlands ES, Blackledge GRP, Slack JA, et al. (1992) Phase I trial of temozolomide (CCRG 81045: M&B 39831: NSC 362856). Br J Cancer 65:287–291
8. Brada M, Judson I, Beale P, et al. (1999) Phase I dose-escalation and pharmacokinetic study of temozolomide (SCH 52365) for refractory or relapsing malignancies. Br J Cancer 81:1022–1030
9. Rudek MA, Donehouwer RC, Statkevich P, et al. (2004) Temozolomide in patients with advanced cancer: phase I and pharmacokinetic study. Pharmacotherapy 24:16–25
10. Beale P, Judson I, Moore S, et al. (1999) Effect of gastric pH on the relative oral bioavailability and pharmacokinetics of temozolomide. Cancer Chemother Pharmacol 44:389–394
11. Kleihues P, Louis DN, Scheithauer BW, et al. (2002) The WHO classification of tumors of the nervous system. J Neuropathol Exp Neurol 61:215–225; discussion 226–229
12. Hammond LA, Eckardt JR, Baker SD, et al. (1999) Phase I and pharmacokinetic study of temozolomide on a daily-for-5-days schedule in patients with advanced solid malignancies. J Clin Oncol 17:2604–2613

Oncogene (2007) 26, 5577–5586

www.nature.com/onc

ORIGINAL ARTICLE

Neuropilin-1 promotes human glioma progression through potentiating the activity of the HGF/SF autocrine pathway

B Hu[1], P Guo[1,2], I Bar-Joseph[1,2], Y Imanishi[1,2], MJ Jarzynka[1,2], O Bogler[3], T Mikkelsen[4], T Hirose[5], R Nishikawa[6] and SY Cheng[1,2]

[1]University of Pittsburgh Cancer Institute & Department of Pathology, Pittsburgh, PA, USA; [2]Department of Pathology, Research Pavilion at Hillman Cancer Center, Pittsburgh, PA, USA; [3]Department of Neurosurgery & Brain Tumor Center, MD Anderson Cancer Center, University of Texas, Houston, TX, USA; [4]Department of Neurosurgery, Hermelin Brain Tumor Center, Henry Ford Hospital, Detroit, MI, USA; [5]Department of Pathology, Saitama Medical University, Saitama, Japan and [6]Department of Neurosurgery, Saitama Medical University, Saitama, Japan

Neuropilin-1 (NRP1) functions as a coreceptor through interaction with plexin A1 or vascular endothelial growth factor (VEGF) receptor during neuronal development and angiogenesis. NRP1 potentiates the signaling pathways stimulated by semaphorin 3A and VEGF-A in neuronal and endothelial cells, respectively. In this study, we investigate the role of tumor cell-expressed NRP1 in glioma progression. Analyses of human glioma specimens (WHO grade I–IV tumors) revealed a significant correlation of NRP1 expression with glioma progression. In tumor xenografts, overexpression of NRP1 by U87MG gliomas strongly promoted tumor growth and angiogenesis. Overexpression of NRP1 by U87MG cells stimulated cell survival through the enhancement of autocrine hepatocyte growth factor/scatter factor (HGF/SF)/c-Met signaling. NRP1 not only potentiated the activity of endogenous HGF/SF on glioma cell survival but also enhanced HGF/SF-promoted cell proliferation. Inhibition of HGF/SF, c-Met and NRP1 abrogated NRP1-potentiated autocrine HGF/SF stimulation. Furthermore, increased phosphorylation of c-Met correlated with glioma progression in human glioma biopsies in which NRP1 is upregulated and in U87MG NRP1-overexpressing tumors. Together, these data suggest that tumor cell-expressed NRP1 promotes glioma progression through potentiating the activity of the HGF/SF autocrine c-Met signaling pathway, in addition to enhancing angiogenesis, suggesting a novel mechanism of NRP1 in promoting human glioma progression.
Oncogene (2007) **26**, 5577–5586; doi:10.1038/sj.onc.1210348; published online 19 March 2007

Keywords: neuropilin-1; HGF/SF; c-Met; glioma

Correspondence: Dr S-Y Cheng, University of Pittsburgh Cancer Institute & Department of Pathology, Suite 2.26, 5117 Centre Avenue; Pittsburgh, PA 15213-1863, USA or Dr B Hu, University of Pittsburgh Cancer Institute & Department of Medicine, Suite 2.26, 5117 Centre Avenue; Pittsburgh, PA 15213-1863, USA.
E-mail: chengs@upmc.edu or hub@upmc.edu
Received 18 September 2006; revised 18 December 2006; accepted 6 January 2007; published online 19 March 2007

Introduction

Neuropilin-1 (NRP1) is a type I cell surface co-receptor that plays important roles in the development of the nervous system and angiogenesis (Bagri and Tessier-Lavigne, 2002). During neuronal development, NRP1-mediated signal transduction requires the formation of a functional semaphorin (Sema) 3A-NRP1-plexin A1 complex, which inhibits axonal guidance signals to the projecting neurons (Bagri and Tessier-Lavigne, 2002). In endothelial cells, NRP1 enhances the interaction of heparin-binding vascular endothelial growth factor $(VEGF)_{165}$ with its receptors (VEGFRs) and modulates VEGF-stimulated angiogenesis. Elevated expression of NRP1 was also found in tumor cells in various types of human cancers (Klagsbrun *et al.*, 2002). Overexpression of NRP1 in prostate and colon cancer cells enhances angiogenesis and tumor growth in animals (Miao *et al.*, 2000; Parikh *et al.*, 2004), whereas expression of an antagonist of NRP1 inhibited vessel growth and tumor expansion (Gagnon *et al.*, 2000).

Hepatocyte growth factor/scatter factor (HGF/SF) modulates various cellular functions such as proliferation, migration and morphogenesis through its cognate surface receptor c-Met (Gao and Vande Woude, 2005). Activation of the HGF/SF/c-Met signaling pathway correlates with the malignancy of human gliomas (Abounader and Laterra, 2005). Overexpression of HGF/SF in glioma cells resulted in enhanced tumorigenicity and growth *in vivo* (Laterra *et al.*, 1997). Inhibition of endogenous HGF/SF and c-Met in human cancer cells, including gliomas, reversed their malignant phenotype (Abounader *et al.*, 2002). Additionally, the activation of signaling molecules such as extracellular signal-regulated kinase (ERK) and Bcl-2 antagonist of cell death (Bad) is involved in the HGF/SF/c-Met pathway in cancer cells (Abounader and Laterra, 2005). NRP1 was recently demonstrated to interact directly with a subset of heparin-binding growth factors, such as fibroblast growth factor-2 (FGF-2), FGF-4 and HGF/SF and potentiates FGF-2 stimulation of endothelial cells (West *et al.*, 2005), suggesting that NRP1 expression in glioma cells may augment

HGF/SF/c-Met stimulation of tumor progression through an autocrine loop.

In this study, we investigated the roles of tumor cell-expressed NRP1 in human glioma progression. We show that upregulated NRP1 is primarily expressed in tumor cells, and NRP1 expression correlates with tumor progression in clinical glioma specimens. We demonstrate that NRP1 expression promotes glioma growth and survival *in vitro* and *in vivo* through an autocrine HGF/SF/c-Met signaling pathway involving activation of c-Met, ERK and Bad, thus suggesting a novel mechanism of NRP1 expression in promoting cancer cell survival and proliferation.

Results

Upregulation of NRP1 is correlated with the malignancy of human astrocytic tumors

To determine the association of NRP1 expression with glioma progression, we performed immunohistochemistry (IHC) analyses on a total of 92 human glioma specimens and four normal human brain biopsies using three well-characterized anti-NRP1 antibodies (Ding *et al.*, 2000) and isotype matched IgGs as negative controls that all showed no staining (see the insets in Figure 1A). As shown in Figure 1Aa, in all four normal brain tissues analysed, weak immunoactivity for the anti-NRP1 antibody was detected in neurons (red arrow) or cells within a blood vessel (arrowhead). In four pilocytic astrocytoma specimens (P.A., WHO grade I), NRP1 was weakly stained in a few tumor cells (Figure 1Ab, arrows) and vessels (panel b, arrowhead). In 24 WHO grade II gliomas, NRP1 protein was detected in tumor cells (panel c, arrows) and vessels (panel c, arrowhead). In 21 WHO grade III glioma biopsies, a greater intensity of NRP1 staining was detected in tumor cells (Figure 1Ad, arrows). In 43 WHO grade IV glioblastoma multiforme (GBM) specimens, high expression of NRP1 was found in tumor cells (Figure 1Ae, arrows). In general, no increase in staining for NRP1 protein was found in hypoxic/pseudopalisading regions, but heterogeneous staining for NRP1 expression was seen within the gliomas. As summarized in Figure 1B and Supplementary Table S1 (Supplementary Material), statistical analyses of our IHC data revealed a significant correlation between NRP1 expression and human glioma progression. There was a significant difference in IHC staining for NRP1 among the three groups as well as a correlation between NRP1 expression and the malignancy of human glioma (Figure 1B).

Overexpression of NRP1 in U87MG xenografts promotes tumor growth and angiogenesis in vivo

To further investigate whether upregulation of NRP1 by glioma cells promotes tumor progression, we first examined expression of NRP1 in human glioma cell lines by immunoblot (IB) analyses. As shown in Figure 2a, NRP1 protein was detected at various levels in all glioma cell lines examined. As U87MG cells express NRP1 at a relatively low level and are highly tumorigenic in mice (Hu *et al.*, 2003), we utilized this cell line to stably overexpress NRP1. Among various U87MG cell clones that stably express NRP1, we chose two cell clones, U87MG/NRP1-no. 1 and U87MG/NRP1-no. 8, that expressed exogenous NRP1 at medium (NRP1-no. 1) or high levels (NRP1-no. 8) compared with U87MG (Figure 2b) or LacZ (see below) cells for further studies. Next, we separately implanted U87MG and NRP1 cells into the flank or the brain of nude mice. On the 26th day post-implantation, inoculation of NRP1 cells into the flank resulted in formation of tumors with an average volume of $1205 \pm 307\,mm^3$, whereas mice that received U87MG or LacZ cells (Guo *et al.*, 2001) developed tumors with similar volumes in 45 days (Figure 3A). In the brain, mice receiving NRP1 cells developed tumors with a volume of $34 \pm 6.8\,mm^3$ in 25 ± 3 days ($n = 17$) (Figure 3Bc, d and 3C), whereas mice inoculated with U87MG or LacZ cells developed tumors of $15 \pm 4.5\,mm^3$ in the same period of time ($n = 15$) (Figure 3Ba, b and 3C). Afterwards, we stained the brain tumor tissue using anti-CD31 (Figure 3Bb and d) and anti-bromodeoxyuridine (BrdUrd) plus anti-von Willebrand factor (vWF) antibodies (Figure 3E). We found that NRP1 intracranial tumors had a 2.5-fold increase in vessel density (Figure 3D) and a 2.6-fold increase in BrdUrd incorporation in the tumor cells when compared with U87MG tumors (Figure 3F).

NRP1 promotes U87MG cell growth through enhancing autocrine HGF/SF/c-Met signaling

Our results show that overexpression of NRP1 by glioma cells enhances tumor cell proliferation *in vivo*, which could possibly be due to NPR1-modulated autocrine intracellular signaling stimulation in glioma cells or caused indirectly by an increase in angiogenesis. To distinguish these possibilities, we performed a trypan blue vital dye exclusion assay. NRP1 overexpression did not significantly affect NRP1 cell growth compared with U87MG or LacZ cells when cultured in medium containing 10% fetal bovine serum (FBS) (data not shown). However, as shown in Figure 4A, in the absence of serum, NRP1 cells showed a 1.8-fold increase in cell survival, whereas U87MG or LacZ cells demonstrated a slight decrease of cell survival in a 4-day culture, suggesting that autocrine signaling through NRP1 promotes cell survival in these glioma cells.

A recent study demonstrated NRP1 also interacts with several heparin-binding growth factors, such as FGF-2, FGF-4 and HGF/SF, and potentiates the growth stimulatory activity of FGF-2 on endothelial cells (West *et al.*, 2005). As HGF/SF and FGF-2 were shown to stimulate cell growth through receptor-mediated autocrine signaling in glioma cells (Abounader and Laterra, 2005), we performed enzyme-linked immunosorbent assay (ELISA) and determined whether the autocrine signaling activities of these growth factors were involved in the NRP1-stimulated U87MG cell survival and growth. In a 48-h cell culture,

A

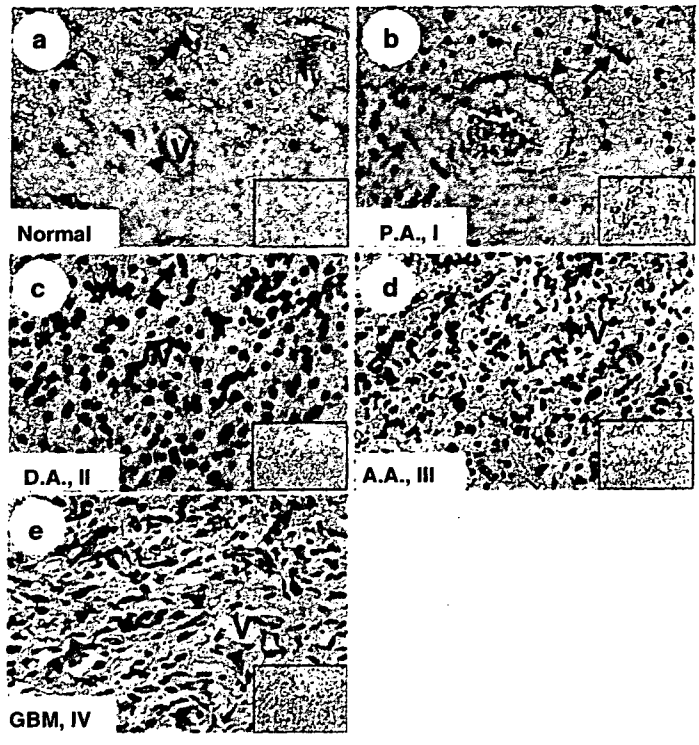

B **NRP-1 Expression Correlates with Human Glioma Progression**

WHO grade	n	Histology	n	Score -	Score ±	Score 1+	Score 2+	Score 3+	Kruskal-Wallis test* with Scheffe's post-hoc test
Normal	4	Normal	4	4	0	0	0	0	Normal+I
I	4	Pilocytic astrocytoma	4	0	4	0	0	0	Normal+I
II	24	Oligodendroglioma	13	2	4	5	2	0	II
		Diffuse astrocytoma	10	0	0	5	5	0	II
		Oligoastrocytoma	1	0	0	1	0	0	II
III	21	Anaplastic astrocytoma	13	0	1	7	5	0	III+IV
		Anaplastic oligodendroglioma	7	0	0	3	3	1	III+IV
		Anaplastic oligoastocytoma	1	0	0	0	1	0	III+IV
IV	43	Glioblastoma multiforme	43	0	3	16	18	6	

Normal+I vs II: $p < 0.01$; II vs III+IV: $p < 0.05$; Normal+I vs III+IV: $p < 0.01$

*Kruskal-Wallis test between Normal+Grade I vs Grade II vs Grade III+IV showed significant difference with $p < 0.00001$. Differences between each group were then examined by Scheffe's post-hoc test and each p-value were indicated in the table.

n, number of specimens. Score, intensity of IHC staining in the clinical specimens by an ant-NRP1-antibody and is defined as described in the Materials and Method section.

Figure 1 NRP1 expression correlates with human glioma progression. (**A**) IHC of paraffin sections of normal human brain (panel a), P.A. (WHO grade I, panel b), diffuse astrocytoma (D.A., grade II, panel c), anaplastic astrocytoma (A.A., grade III, panel d) and GBM (grade IV, panel e) tissue. Insets in panels a–e are the isotype-matched IgG control staining of identical areas. Arrows indicate neurons (a) or tumor cells (b to e) that are positive for NRP1. Arrowheads indicate endothelial cells in tumor-associated vessels that express NRP1. Results are representative of three independent experiments. Original magnification: × 400. (**B**) Statistical analyses. A total of 92 individual primary tumor specimens (WHO grade I–IV) and four normal human brain biopsies were analysed.

U87MG, LacZ and NRP1 cells secreted VEGF (30 ± 3.6 ng/ml/10^6 cells), FGF-2 (14 ± 2.1 pg/ml/10^6 cells) and HGF/SF (400 ± 45 pg/ml/10^6 cells) into serum-free medium at similar levels. A neutralizing anti-HGF/SF antibody abolished the effect of NRP1-enhanced U87MG cell survival, whereas neutralizing anti-FGF-2 and anti-VEGF antibodies had little or no effect on cell survival of U87MG and NRP1 cells (Figure 4B).

To investigate whether the HGF/SF/c-Met signaling pathway mediates NRP1 stimulation of glioma cells, we examined the expression and tyrosine phosphorylation

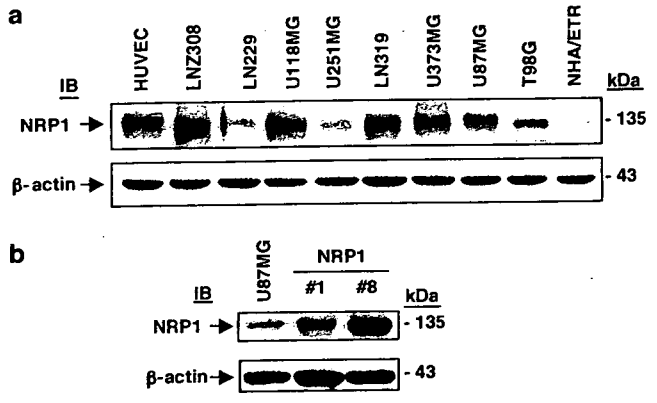

Figure 2 Overexpression of NRP1 in U87MG glioma cells. IB analyses of HUVEC, NHA/ETR and various glioma cell lines (**a**) or U87MG and NRP1-no. 1 and NRP1-no. 8 cells (**b**) using a polyclonal anti-NRP1 antibody (C-18). β-Actin was used as a loading control. Similar results were also obtained using a polyclonal anti-NRP1 antibody (NP1ECD1A). Results are representative of three independent experiments.

of c-Met in U87MG and NRP1 cells in the absence or presence of the HGF/SF neutralizing antibody. As shown in Figure 4C, in the absence of serum, expression of endogenous c-Met was not enhanced by NRP1 overexpression, but tyrosine phosphorylation of c-Met was stimulated in NRP1 but not U87MG or LacZ cells. When the HGF/SF neutralizing antibody was included in the cell culture, the NRP1-induced phosphorylation of c-Met was diminished. As U87MG, LacZ and NRP1 cells secrete low levels of endogenous HGF/SF in the serum-free CM (400 ± 45 pg/ml/10^6 cells) and no inhibitory effect of the neutralizing anti-HGF/SF on U87MG parental cell survival (Figure 4B) was seen, we reasoned that the HGF/SF/c-Met autocrine signaling pathway was not activated due to low levels of the endogenous HGF/SF in U87MG or LacZ cells. Furthermore, NRP1 overexpression in U87MG cells potentiated HGF/SF/c-Met autocrine signaling by activating a downstream target, Bad, an antiapoptotic molecule (Abounader and Laterra, 2005) (Figure 4C). Phosphorylation of Bad at Ser-112 was induced by NRP1 overexpression, but only a slight enhancement occurred on the constitutively phosphorylated Ser-136 of Bad. Additionally, a 4-day culture in serum-free medium did not alter the expression levels of NRP1 in U87MG, LacZ or NRP1-expressing cells (Figure 4D).

Although U87MG cells are deficient in plexin A1 and VEGFR-2, Sema 3A, a cognate ligand for NRP1, is expressed in U87MG cells (Rieger *et al.*, 2003). Thus, we tested a specific knockdown of Sema 3A by siRNA to examine the effects of endogenous Sema 3A on NRP1-enhanced U87MG cell growth. As shown in Figure 4E, endogenous c-Met (panel a) and Sema 3A (panel b) were considerably suppressed compared with the control siRNA-transfected cells. Reduced expression of c-Met, but not Sema 3A, in NRP1 cells significantly abolished the NRP1-enhanced U87MG cell survival (Figure 4F).

NRP1 potentiates glioma cell proliferation in response to exogenous HGF/SF

We assessed whether NRP1 overexpression could potentiate stimulation of glioma cell proliferation by exogenous HGF/SF using a BrdUrd incorporation assay. As shown in Figure 5A, in the absence of recombinant human (rh) HGF/SF, the basal level of BrdUrd incorporation in NRP1-no. 1 and -no. 8 cells was similar to that in U87MG and LacZ cells. When cells were treated with 5 or 10 ng/ml of rhHGF/SF, a significant increase in BrdUrd incorporation was found in NRP1-no. 1 and -no. 8 cells compared with U87MG and LacZ cells, whereas stimulation by 25 ng/ml rhHGF/SF markedly enhanced BrdUrd incorporation in U87MG and LacZ cells. Further increases of rhHGF/SF (50 or 75 ng/ml) had no further augmentation of BrdUrd incorporation in U87MG, LacZ and NRP1 cells. Also, NRP1-potentiated cell proliferation was proportional to the level of exogenous NRP1 expression in the glioma cells when comparing the BrdUrd incorporation level in NRP1-no. 8 cells (higher level of exogenous NRP1) to NRP1-no. 1 cells (lower level of NRP1 expression, Figure 2b).

Next, we assessed the activation of c-Met and two of its downstream effectors, ERK and Bad. As shown in Figure 5B, when cells were treated with 10 ng/ml rhHGF/SF for 20 or 40 min, phosphorylation of ERK1/2 and Bad at Ser-112 was evident in NRP1-expressing cells but not in LacZ cells. Moreover, treatment with 25 μmol/l U0126, a specific inhibitor for ERK, inhibited HGF/SF-stimulated phosphorylation of ERK and Bad as well as BrdUrd incorporation in NRP1 cells but not in LacZ cells (Figure 5Ca and b). To a similar extent, suppression of Bad protein expression in these cells by a specific siRNA (Figure 5Da) also significantly attenuated HGF/SF-stimulated BrdUrd incorporation in NRP1 cells but had no effect on LacZ cells or untreated cells (Figure 5Db).

To further confirm the critical role of NRP1 expression on potentiation of HGF/SF/c-Met signaling, we determined the effects of endogenous NRP1 on cell growth in LNZ-308 glioma cells, as LNZ-308 cells express endogenous NRP1 at high levels (Figure 2a) and no endogenous HGF/SF protein was detected by ELISA in serum-free CM (data not shown). As shown in Figure 6a, three individual siRNAs for NRP1 (N1, N2 and N3) suppressed endogenous NRP1 protein at various levels in LNZ-308 cells, whereas a pool of these three siRNAs for NRP1 (N1:N2:N3 = 1:1:1) considerably suppressed endogenous NRP1 protein. When control siRNA-transfected LNZ-308 cells were stimulated with rhHGF/SF, BrdUrd incorporation increased by 1.6-fold in response to 10 ng/ml of rhHGF/SF and reached a peak when 20 ng/ml HGF/SF was used (Figure 6b). Stimulation by HGF/SF on LNZ-308 cells at higher concentrations (60 and 80 ng/ml) had no further effect (Figure 6b). Importantly, when endogenous NRP1 expression was inhibited using siRNA, HGF/SF-stimulated BrdUrd incorporation at low concentrations (10 and 20 ng/ml) was significantly attenuated.

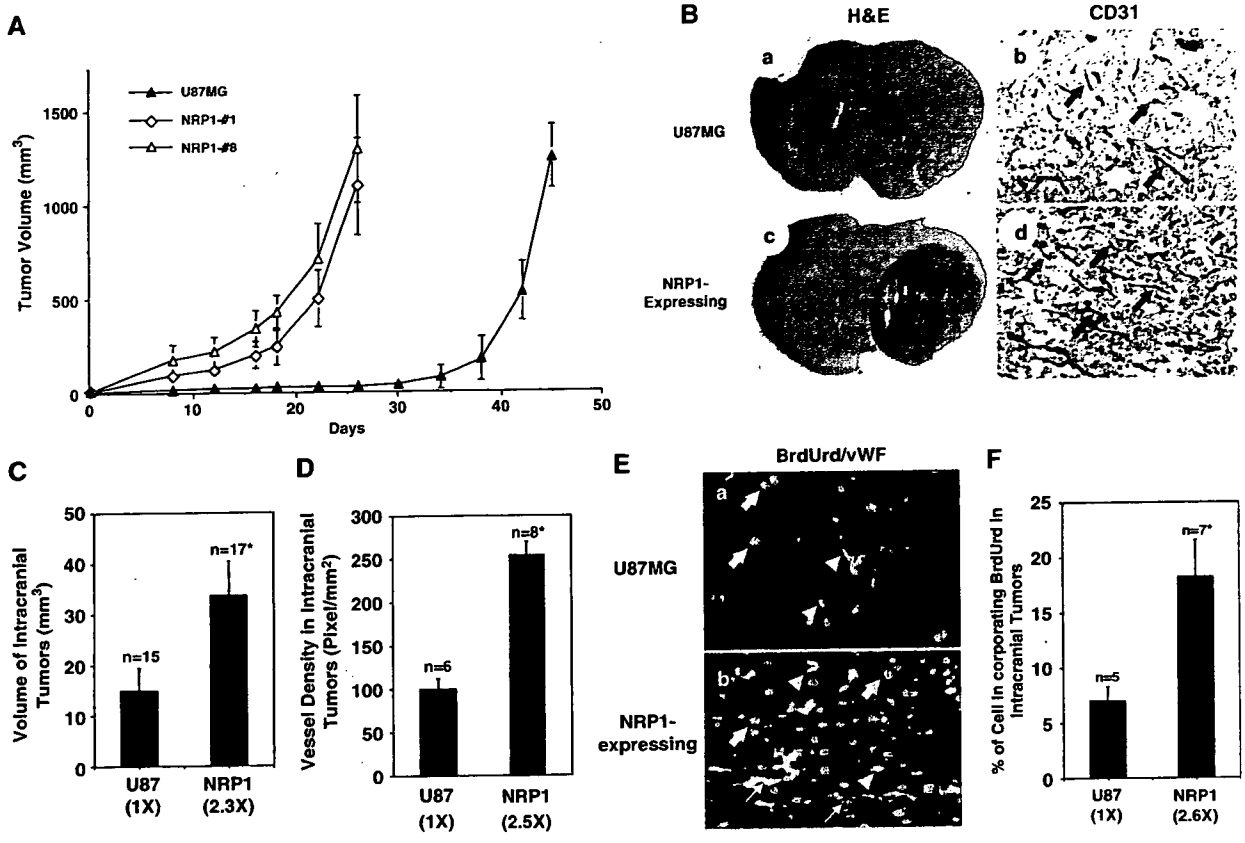

Figure 3 Overexpression of NRP1 in U87MG cells promotes tumor growth and angiogenesis. (**A**) Growth kinetics of U87MG or NRP1 tumors at subcutaneous sites. Tumor volume was estimated (volume = $(a^2 \times b)/2$, $a<b$) using a caliper at the indicated times. Data are shown as mean ± s.d. (**B**) Tumorigenicity and angiogenesis of U87MG brain tumors. IHC analyses are shown for U87MG (panels a and b) or NRP1 (c and d) gliomas. Panels a and c are brain sections stained with hematoxylin and eosin (H&E). Panels b and d show CD31 staining for tumor vessels. Arrows in a and c, tumor mass. Arrows in b and d, blood vessels. Five to eight individual tumor samples of each group from each *in vivo* experiment were analysed. Original magnification: panels a and c, × 12.5; b and d, × 200. (**C**) and (**D**) Quantitative analyses of tumorigenesis and angiogenesis in various intracranial tumors. Data are means ± s.d. Numbers in parentheses, the difference in fold between U87MG and NRP1 gliomas. (**E**) and (**F**) Cell proliferation of various intracranial gliomas. (**E**) IHC staining of U87MG brain tumors with a monoclonal anti-BrdUrd antibody (red) together with a polyclonal anti-vWF antibody (green). Blue arrows, proliferative nuclei in tumor cells. White arrows, proliferative nuclei of blood vessels. Blue arrowheads, vWF staining of vessels. Three to five serial sections from five to seven individual samples of each tumor type were analysed. Original magnification: × 400. (**F**) Quantitative analyses of cellular BrdUrd incorporation in U87MG and U87MG/NRP1 tumors. Numbers in parentheses, the difference in fold between U87MG/NRP1 and parental U87MG gliomas. Results in (**A–E**) are representative of three independent experiments.

Next, we examined activation of the HGF/SF/c-Met signaling pathway in various siRNA-transfected LNZ-308 cells in response to HGF/SF stimulation. As shown in Figure 6c, HGF/SF stimulation at 10, 25 and 50 ng/ml induces phosphorylation of c-Met, Erk1/2 and Bad. When NRP1 expression was suppressed using siRNA, the activation by HGF/SF at 10 and 25 ng/ml on c-Met, ERK1/2 and Bad was diminished. No inhibitory effect on HGF/SF stimulation was seen when NRP1 siRNA-transfected LNZ-308 cells were treated with 50 ng/ml HGF/SF.

NRP1 enhances HGF/SF/Met signaling in human glioma

Next, we sought to determine whether activation of c-Met also occurred in NRP1-expressing tumors *in vivo*. We extracted tissue lysates from U87MG and NRP1 tumors and performed IB analysis. As shown in Figure 7a, NRP1 overexpression did not increase c-Met expression in the NRP1 tumors. However, increased phosphorylation of c-Met was detected in the tissue lysates of NRP1 tumors compared with the parental tumors established at subcutaneous and orthotopic sites. Finally, we examined whether increased expression of NRP1 and c-Met phosphorylation correlates with glioma progression in 14 primary human glioma tissue samples by IB analyses. As shown in Figure 7b, c-Met was detected at various levels in all of the glioma tissues, whereas upregulation of NRP1 expression was seen primarily in high-grade tumors (grades III and IV). Importantly, c-Met phosphorylation was also increased in high-grade gliomas, mostly in grade IV GBM specimens, correlating with the expression profile of NRP1 in these clinical samples.

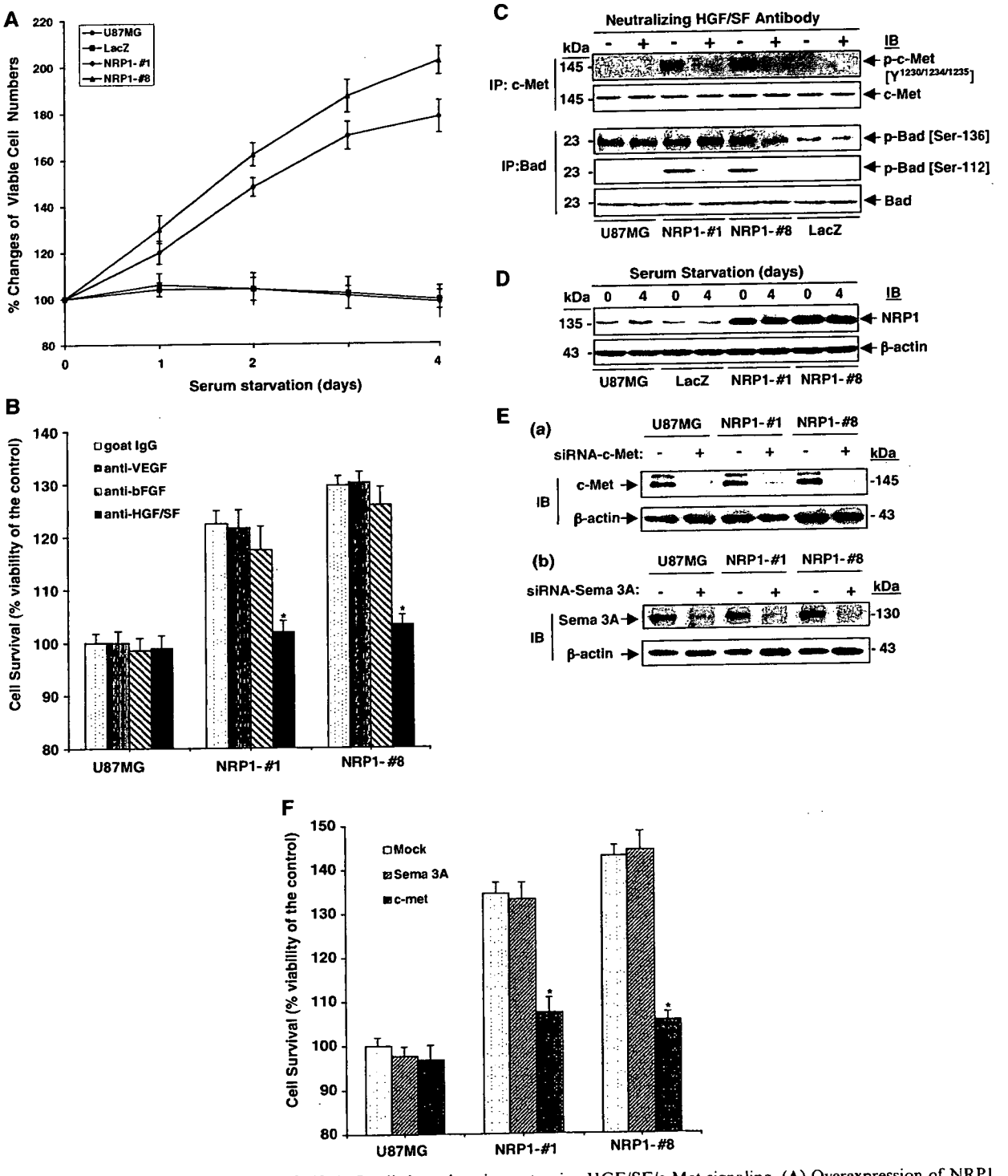

Figure 4 NRP1 promotes survival of U87MG cells by enhancing autocrine HGF/SF/c-Met signaling. (**A**) Overexpression of NRP1 promotes U87MG cell survival. Data of cell survival assays are shown as mean ± s.d. (**B**) Inhibition of HGF/SF, but not FGF-2 or VEGF, suppresses NRP1-promoted U87MG cell survival. Data of cell survival assays are shown as mean ± s.d. (**C**) Inhibition of tumor cell-derived HGF/SF, but not VEGF or FGF-2, suppresses NRP1-potentiated activation of c-Met and Bad. IP and IB analyses of various U87MG cells treated with or without the HGF/SF neutralizing antibody. (**D**) Serum starvation did not alter NRP1 expression in U87MG, LacZ and NRP1 cells. IB analyses of various cell lysates under the same conditions as in (**A**). (**E**) and (**F**) Inhibition of endogenous c-Met but not Sema 3A attenuates NRP1-potentiated U87MG cell viability. (**E**) Suppression of endogenous c-Met and Sema 3A by siRNA. IB analyses of c-Met and Sema 3A proteins in various U87MG cells. (**F**) Cell survival assays of siRNA-transfected U87MG and NRP1 cells. Data are shown as mean ± s.d. In (**B–D**), c-Met, Bad and β-actin were used as loading controls. Results in (**A–F**) are representative of three independent experiments.

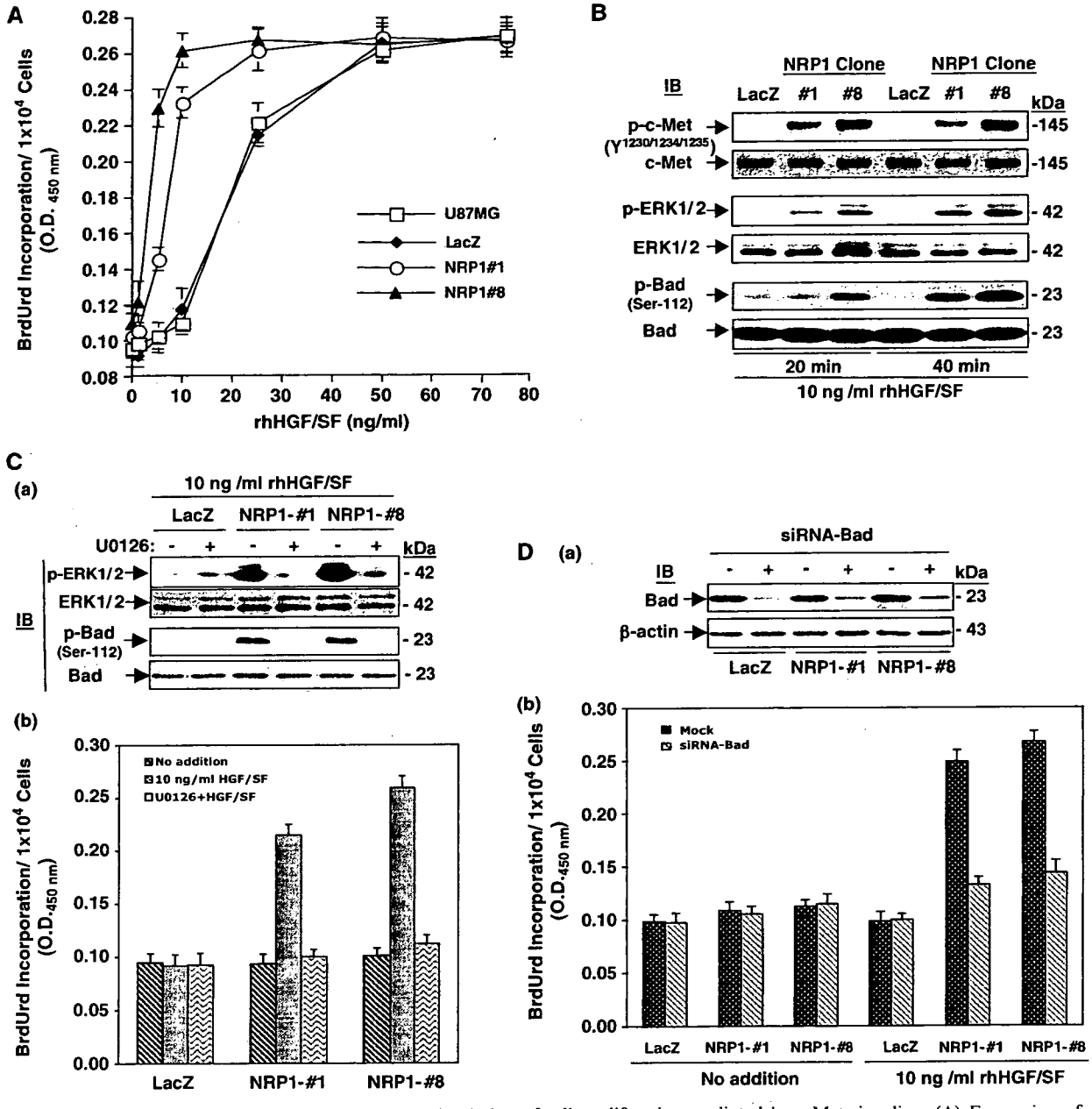

Figure 5 NRP1 expression potentiates HGF/SF stimulation of cell proliferation mediated by c-Met signaling. (**A**) Expression of NRP1 in U87MG cells potentiates cell proliferation in response to a low dose of HGF/SF stimulation. Data of BrdUrd incorporation in U87MG, LacZ, NRP1-no. 1, and NRP1-no. 8 cells are shown as mean±s.d. (**B**) IB analyses of NRP1-potentiated HGF/SF stimulation of phosphorylation on c-Met, ERK1/2 and Bad in various U87MG cells. (**C**) U0126 attenuated NRP1-potentiated HGF/SF stimulation of phosphorylation on ERK1/2 and Bad (panel a, IB analyses) and cell proliferation in various U87MG cells (panel b, BrdUrd incorporation assays; data are shown as mean±s.d.). (**D**) Knockdown of Bad by siRNA (panel a, IB analyses) attenuates NRP1-potentiated HGF/SF stimulation of cell proliferation in various U87MG cells (panel b, data are shown as mean±s.d.). In (**B–D**), c-Met, ERK1/2, Bad and β-actin were used as loading controls. Results in (**A**) to (**D**) are representative of three independent experiments.

Discussion

The role of NRP1 in human tumor progression has been studied in various cancer model systems. Upregulation of NRP1 was found not only in endothelia but also in tumor cells in various types of primary human cancer specimens (Ding *et al.*, 2000; Akagi *et al.*, 2003). Overexpression of NRP1 in tumor cells has been shown to promote tumor growth and angiogenesis in xenograft models and cell survival in cancer cells. In these reports, NRP1 stimulation of tumor progression was primarily attributed to VEGF-dependent pathways (Miao *et al.*, 2000; Bachelder *et al.*, 2003). This study provides new evidence that glioma cell-expressed NRP1 promotes tumor progression through potentiating the HGF/SF/c-Met signaling pathway. We show in primary human

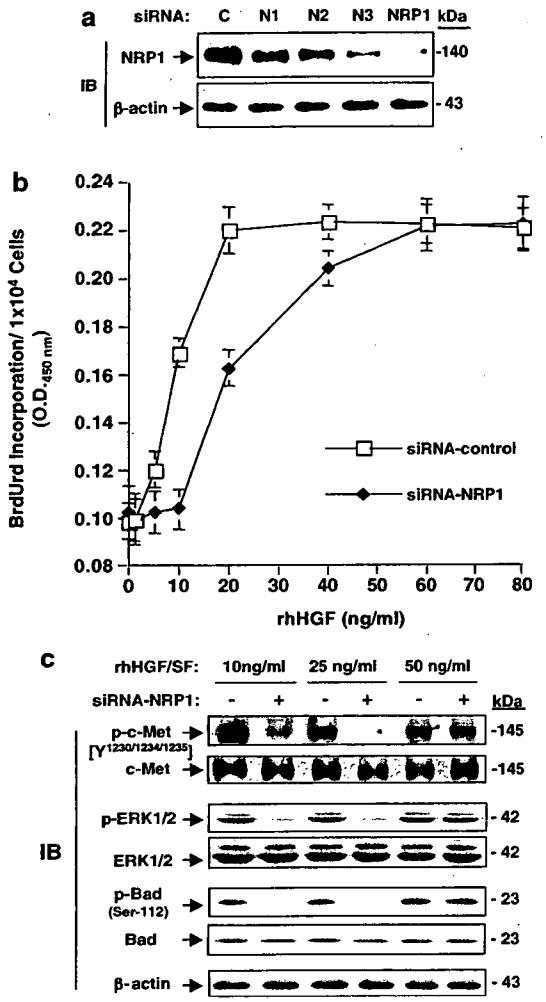

Figure 6 Inhibition of endogenous NRP1 attenuated HGF/SF stimulation of cell proliferation and HGF/SF/c-Met signaling in LNZ-308 glioma cells. (**a**) Inhibition of endogenous NRP1 by NRP1/siRNA in LNZ-308 cells detected by IB analyses. C, control siRNA. N1, N2 and N3, individual siRNAs for NRP1. NRP1, a pool of all three siRNAs of N1, N2 and N3. β-Actin was used as a loading control. (**b**) Inhibition of endogenous NRP1 in LNZ-308 cells using siRNA-attenuated rhHGF/SF stimulation of cell proliferation. Data of BrdUrd incorporation of siRNA-transfected LnZ-308 cells are shown as mean ± s.d. (**c**) Inhibition of endogenous NRP1 in LNZ-308 cells using siRNA-suppressed HGF/SF stimulation of c-Met signaling detected by IB analyses. c-Met, ERK1/2 Bad and β-actin were used as loading controls. Results in (**a**–**c**) are representative of three independent experiments.

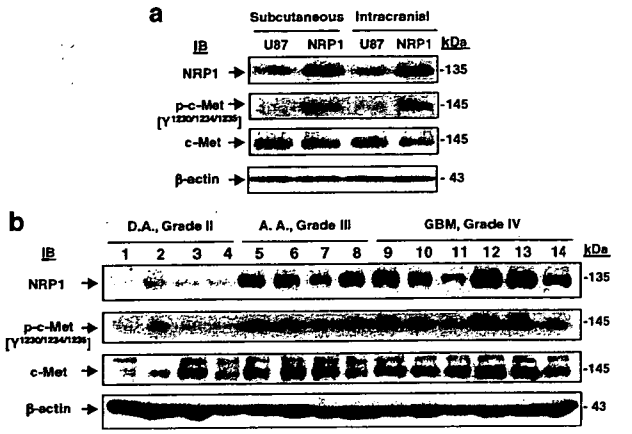

Figure 7 Upregulation of NRP1 correlates with the activation of c-Met in U87MG tumor xenografts and in high-grade human glioma specimens. (**a**) Overexpression of NRP1 in U87MG xenografts resulted in activation of c-Met in the established tumors. IB analyses of U87MG and NRP1 xenografted tumors. β-Actin was used as a loading control. (**b**) Upregulation of NRP1 expression correlates with activation of c-Met during glioma progression. IB analyses of 14 frozen primary human glioma specimens. c-Met and β-actin were used as loading controls. Results are representative of three independent experiments.

glioma specimens that upregulation of tumor cell-expressed NRP1 correlates with glioma progression and increased activation of c-Met in these clinical tumor samples. We demonstrated that overexpression of NRP1 by U87MG glioma cells enhanced tumor growth in mice through potentiating HGF/SF/c-Met activity stimulating tumor cell proliferation in mice. NRP1 potentiated the autocrine HGF/SF/c-Met signaling pathway in response to low concentrations of HGF/SF *in vitro*, and NRP1 expression is also correlated with c-Met activation in U87MG tumors that overexpress NRP1. Conversely, inhibition of tumor cell-derived HGF/SF, but not FGF-2 or VEGF, by neutralizing antibodies and of endogenous c-Met, but not Sema 3A, by specific siRNAs attenuates HGF/SF/c-Met signaling and glioma cell viability. Furthermore, suppression of endogenous NRP1 in LNZ-308 cells abolishes exogenous HGF/SF stimulation of c-Met-mediated signaling in the tumor cells at lower concentrations. Our results corroborate a recent study showing that overexpression of NRP1 in human pancreatic cancer cells resulted in constitutive activation of mitogen-activated protein kinase signaling (Wey *et al.*, 2005). A plausible mechanism of NRP1 stimulation of tumor progression in our study and the pancreatic cancer model is that NRP1 enhances endogenous signaling modulating tumor cell function independent of VEGF. Our results of NRP1 potentiation of the HGF/SF/c-Met signaling pathway in glioma cells agree with another recent study showing that that NRP1 not only interacts directly with multiple heparin-binding growth factors, such as FGF-2, FGF-4 and HGF/SF, but also potentiates stimulation of FGF-2 on endothelial cells (West *et al.*, 2005). In addition, the increased sensitivity to HGF/SF/c-Met signaling by endogenously expressed NRP1 in glioma cells is analogous to the increase in sensitivity to FGF-2 caused by the addition of a soluble NRP1 dimer to endothelial cells in the aforementioned study. Expression of NRP1 in various cell types may sensitize the cells to their microenvironments, thereby potentiating the corresponding intracellular signaling critical for cellular function.

Increased expression of NRP1 has been detected in tumor cells in clinical glioma samples, suggesting a link between NRP1 expression and glioma malignancy (Ding *et al.*, 2000). Our results further elaborate on these observations. By analysing a total of 92 primary human

glioma specimens, we show that upregulation of NRP1 in tumor cells correlates with glioma progression. In U87MG tumor xenografts, overexpression of NRP1 markedly stimulated angiogenesis at both anatomic sites (Figure 3). Significant stimulation of vessel growth by tumor cell–expressed NRP1 in our U87MG xenografts and in prostate and colon cancer models (Miao *et al.*, 2000) led to a hypothesis that tumor cell-expressed NRP1 stimulates vessel growth through a juxtacrine mechanism that forms a complex of NRP1 (in tumor cells), VEGF within the tumor microenvironment (intercellular) and VEGFR-2 (in endothelial cells), thus potentiating VEGF activity that enhances angiogenesis and tumor growth (Klagsbrun *et al.*, 2002). However, it is difficult to dissect the NRP1-stimulated juxtacrine signaling in harvested tumor tissues. Nonetheless, these data and the aforementioned studies suggest a far wider spectrum of activity of NRP1 in promoting tumor progression than is currently appreciated.

In summary, this study provides a novel mechanism that expression of NRP1 in human glioma cells promotes glioma progression through potentiating the activity of HGF/SF/c-Met autocrine pathways. Upregulation of NRP1 in tumor cells correlates with the activation of HGF/SF/c-Met pathways in both primary glioma specimens and xenograft gliomas, and inhibition of endogenous c-Met or NRP1 attenuates NRP1-enhanced HGF/SF/c-Met signaling. In addition, our data demonstrating NRP1 expression patterns in primary human glioma specimens and significant enhancement of tumor angiogenesis in glioma xenografts suggest that tumor cell-derived NRP1 stimulates vessel growth in a juxtacrine manner. These pathways appear to act in concert in promoting glioma growth and angiogenesis. Thus, our studies demonstrate a necessity for simultaneously targeting NRP1/VEGF and HGF/SF/c-Met signaling pathways in the treatment of human gliomas.

Materials and methods

Cell lines and their cultures

Human glioma cell lines U87MG, U118MG and T98G were obtained from the American Type Culture Collection (Manassas, VA, USA). Human glioma cell lines U251MG, U373MG, LNZ-308, LN229 and LN319 were from our collection. The transformed normal human astrocytes that form WHO grade III-like glioma in the murine brain (NHA/ETR) were from Dr R Pieper. Human umbilical endothelial cells (HUVEC) were from Cambrex (Rockland, ME, USA). The cells were cultured as described previously (Guo *et al.*, 2001).

siRNA transient transfection

siRNAs were synthesized by Dharmacon Inc. (Lafayette, CO, USA). The sequences of siRNA for target genes were Met, 5′-GTGCAGTATCCTCTGACAG-3′; Sema 3A, 5′-AAAGTTC ATTAGTGCCCACCT-3′ and NRP1 N1, 5′-GAGAGGTCC TGAATGTTCC-3′, N2, 5′-AAGCTCTGGGCATGGAATC AG-3′, and N3, 5′-AAAGCCCCGGGTACCTTACAT-3′; and Bad, Signal Silence Bad siRNA kit (Cell Signaling, Beverly, MA, USA). Cells were transfected with 120 nM of the indicated siRNA or a control siRNA (Invitrogen) using the Oligofectamine reagent (Invitrogen Inc., Carlsbad, CA, USA). After 24 h, siRNAs were removed and the cells were maintained in medium containing 10% FBS for an additional 48 h. The inhibition of protein expression was assessed by IB analysis.

Other methods

Reagents, antibodies, analyses of primary human glioma specimens, IHC, statistics, glioma xenograft models, immunoprecipitation (IP), IB, *in vivo* BrdUrd labeling, generation of U87MG NRP1-expressing cell lines and cell survival and proliferation assays are described in the Supplementary Information.

Acknowledgements

The work was supported by grants NIH CA102011 and RSG CSM-107144 (S-Y C), the Hillman Fellows Program for Innovative Cancer Research to S-Y C and B H, and grant NIH CA095809 to TM (in part).

References

Abounader R, Lal B, Luddy C, Koe G, Davidson B, Rosen EM *et al.* (2002). *In vivo* targeting of SF/HGF and c-met expression via U1snRNA/ribozymes inhibits glioma growth and angiogenesis and promotes apoptosis. *FASEB J* **16**: 108–110.

Abounader R, Laterra J. (2005). Scatter factor/hepatocyte growth factor in brain tumor growth and angiogenesis. *Neuro-oncol* 7: 436–451.

Akagi M, Kawaguchi M, Liu W, McCarty MF, Takeda A, Fan F *et al.* (2003). Induction of neuropilin-1 and vascular endothelial growth factor by epidermal growth factor in human gastric cancer cells. *Br J Cancer* **88**: 796–802.

Bachelder RE, Lipscomb EA, Lin X, Wendt MA, Chadborn NH, Eickholt BJ *et al.* (2003). Competing autocrine pathways involving alternative neuropilin-1 ligands regulate chemotaxis of carcinoma cells. *Cancer Res* **63**: 5230–5233.

Bagri A, Tessier-Lavigne M. (2002). Neuropilins as Semaphorin receptors: *in vivo* functions in neuronal cell migration and axon guidance. *Adv Exp Med Biol* **515**: 13–31.

Ding H, Wu X, Roncari L, Lau N, Shannon P, Nagy A *et al.* (2000). Expression and regulation of neuropilin-1 in human astrocytomas. *Int J Cancer* **88**: 584–592.

Gagnon ML, Bielenberg DR, Gechtman Z, Miao HQ, Takashima S, Soker S *et al.* (2000). Identification of a natural soluble neuropilin-1 that binds vascular endothelial growth factor: *in vivo* expression and antitumor activity. *Proc Natl Acad Sci USA* **97**: 2573–2578.

Gao CF, Vande Woude GF. (2005). HGF/SF-Met signaling in tumor progression. *Cell Res* **15**: 49–51.

Guo P, Xu L, Pan S, Brekken RA, Yang ST, Whitaker GB *et al.* (2001). Vascular endothelial growth factor isoforms display distinct activities in promoting tumor angiogenesis at different anatomic sites. *Cancer Res* **61**: 8569–8577.

Hu B, Guo P, Fang Q, Tao HQ, Wang D, Nagane M *et al.* (2003). Angiopoietin-2 induces human glioma invasion through the activation of matrix metalloprotease-2. *Proc Natl Acad Sci USA* **100**: 8904–8909.

Klagsbrun M, Takashima S, Mamluk R. (2002). The role of neuropilin in vascular and tumor biology. *Adv Exp Med Biol* **515**: 33–48.

Laterra J, Rosen E, Nam M, Ranganathan S, Fielding K, Johnston P. (1997). Scatter factor/hepatocyte growth factor expression enhances human glioblastoma tumorigenicity and growth. *Biochem Biophys Res Commun* **235**: 743–747.

Miao HQ, Lee P, Lin H, Soker S, Klagsbrun M. (2000). Neuropilin-1 expression by tumor cells promotes tumor angiogenesis and progression. *FASEB J* **14**: 2532–2539.

Parikh AA, Fan F, Liu WB, Ahmad SA, Stoeltzing O, Reinmuth N *et al.* (2004). Neuropilin-1 in human colon cancer: expression, regulation, and role in induction of angiogenesis. *Am J Pathol* **164**: 2139–2151.

Rieger J, Wick W, Weller M. (2003). Human malignant glioma cells express semaphorins and their receptors, neuropilins and plexins. *Glia* **42**: 379–389.

West DC, Rees CG, Duchesne L, Patey SJ, Terry CJ, Turnbull JE *et al.* (2005). Interactions of multiple heparin binding growth factors with neuropilin-1 and potentiation of the activity of fibroblast growth factor-2. *J Biol Chem* **280**: 13457–13464.

Wey JS, Gray MJ, Fan F, Belcheva A, McCarty MF, Stoeltzing O *et al.* (2005). Overexpression of neuropilin-1 promotes constitutive MAPK signalling and chemoresistance in pancreatic cancer cells. *Br J Cancer* **93**: 233–241.

Supplementary Information accompanies the paper on the Oncogene website (http://www.nature.com/onc).

ELMO1 and Dock180, a Bipartite Rac1 Guanine Nucleotide Exchange Factor, Promote Human Glioma Cell Invasion

Michael J. Jarzynka,[1,2] Bo Hu,[1,3] Kwok-Min Hui,[1,2] Ifat Bar-Joseph,[1,2] Weisong Gu,[4] Takanori Hirose,[5] Lisa B. Haney,[7] Kodi S. Ravichandran,[7] Ryo Nishikawa,[6] and Shi-Yuan Cheng[1,2]

[1]Cancer Institute and Departments of [2]Pathology and [3]Medicine, University of Pittsburgh, Pittsburgh, Pennsylvania; [4]Ohio Supercomputer Center-Springfield, Springfield, Ohio; Departments of [5]Pathology and [6]Neurosurgery, Saitama Medical University, Moroyama-machi, Iruma-gun, Saitama, Japan; and [7]Beirne Carter Center for Immunology Research and Department of Microbiology, University of Virginia, Charlottesville, Virginia

Abstract

A distinct feature of malignant gliomas is the intrinsic ability of single tumor cells to disperse throughout the brain, contributing to the failure of existing therapies to alter the progression and recurrence of these deadly brain tumors. Regrettably, the mechanisms underlying the inherent invasiveness of glioma cells are poorly understood. Here, we report for the first time that engulfment and cell motility 1 (ELMO1) and dedicator of cytokinesis 1 (Dock180), a bipartite Rac1 guanine nucleotide exchange factor (GEF), are evidently linked to the invasive phenotype of glioma cells. Immunohistochemical analysis of primary human glioma specimens showed high expression levels of ELMO1 and Dock180 in actively invading tumor cells in the invasive areas, but not in the central regions of these tumors. Elevated expression of ELMO1 and Dock180 was also found in various human glioma cell lines compared with normal human astrocytes. Inhibition of endogenous ELMO1 and Dock180 expression significantly impeded glioma cell invasion *in vitro* and in brain tissue slices with a concomitant reduction in Rac1 activation. Conversely, exogenous expression of ELMO1 and Dock180 in glioma cells with low level endogenous expression increased their migratory and invasive capacity *in vitro* and in brain tissue. These data suggest that the bipartite GEF, ELMO1 and Dock180, play an important role in promoting cancer cell invasion and could be potential therapeutic targets for the treatment of diffuse malignant gliomas. [Cancer Res 2007;67(15):7203–11]

Introduction

The inherent invasive nature of malignant gliomas contributes to the high frequency of tumor recurrence and disease progression in patients afflicted with these deadly cancers. In spite of the use of multimodal therapies including surgery, radiation, and chemotherapy, the mean survival time in patients with high-grade gliomas is less than 1 year (1). It is established that the mechanisms regulating cell migration are fundamental to the invasive phenotype of gliomas (2). Although studies show that various stimuli promote glioma cell invasion, the mechanisms underlying dysregulation of cell motility during invasion of these tumor cells remain largely unknown.

Cell migration is highly regulated by spatial and temporal changes of the actin cytoskeleton essential for many physiologic and pathologic processes including cancer cell invasion. Rac1, a member of the Rho GTPase family, is a key regulator of actin cytoskeletal dynamics and relays signals from various stimuli such as growth factors, cytokines, and adhesion molecules to downstream effectors modulating cell migration and invasion (3). Importantly, Rac1 has been shown to promote glioma cell migration (4–10). The activation of Rac1 is through a GDP/GTP exchange mechanism catalyzed by the guanine nucleotide exchange factors (GEF) resulting in an active, GTP-bound state (11). The Rho GTPase GEFs are a large family of proteins that contain either a Dbl homology domain involved in nucleotide exchange (12) or a newly characterized Docker domain that facilitates GEF function (13), of which Dock180 (dedicator of cytokinesis 180) is the prototypical mammalian member.

Dock180 was first identified as a CrkII-binding protein that regulates NIH 3T3 cell morphology (14). Studies in *C. elegans* and *Drosophila* reveal that Dock180 homologues modulate various functions such as phagocytosis, cell migration, myoblast fusion, dorsal closure, and cytoskeletal organization through the activation of Rac1 (15–18). Furthermore, Dock180 stimulates phagocytosis and filopodia formation downstream of integrin receptor signaling in mammalian cells (19, 20). Importantly, Dock180 facilitates nucleotide exchange on Rac1 through its unconventional Docker GEF domain (21–23) but requires binding to engulfment and cell motility 1 (ELMO1) in achieving GDP/GTP exchange on Rac (21). In mammalian cells and in *C. elegans*, ELMO1 and its homologue, CED-12, enhance phagocytosis and cell migration by forming a complex with Dock180 (24). This bipartite GEF complex synergistically functions upstream of Rac1, promoting Rac-dependent cell migration (25). Although ELMO1 and Dock180 stimulate cell migration in normal mammalian cells, whether these molecules play a critical role in cancer cell migration and invasion has not been investigated.

In this study, we show for the first time that ELMO1 and Dock180 stimulate glioma cell migration and invasion. We detected high-level expression of ELMO1 and Dock180 in actively infiltrating glioma cells within the invasive regions along blood vessels, neuronal structures, and the corpus callosum as compared with the central tumor areas of primary human glioma specimens representing WHO grades 2 to 4. Furthermore, we found that ELMO1 and Dock180 expression is increased in human glioma cell lines compared with normal human astrocytes. Inhibition of

Note: Supplementary data for this article are available at Cancer Research Online (http://cancerres.aacrjournals.org/).

Current address for W. Gu: SuperArray Bioscience, 7320 Executive Park, Frederick, MD 21704.

Requests for reprints: Shi-Yuan Cheng, Cancer Institute and Department of Pathology, University of Pittsburgh, HCCLB, 2.26f, 5117 Centre Avenue, Pittsburgh, PA 15213. Phone: 412-623-3261; Fax: 412-623-4840; E-mail: chengs@upmc.edu or Bo Hu, Cancer Institute and Department of Medicine, University of Pittsburgh, HCCLB, 2.19f, 5117 Centre Avenue, Pittsburgh, PA 15213. Phone: 412-623-7791; Fax: 412-623-4840; E-mail: hub@upmc.edu.

doi:10.1158/0008-5472.CAN-07-0473

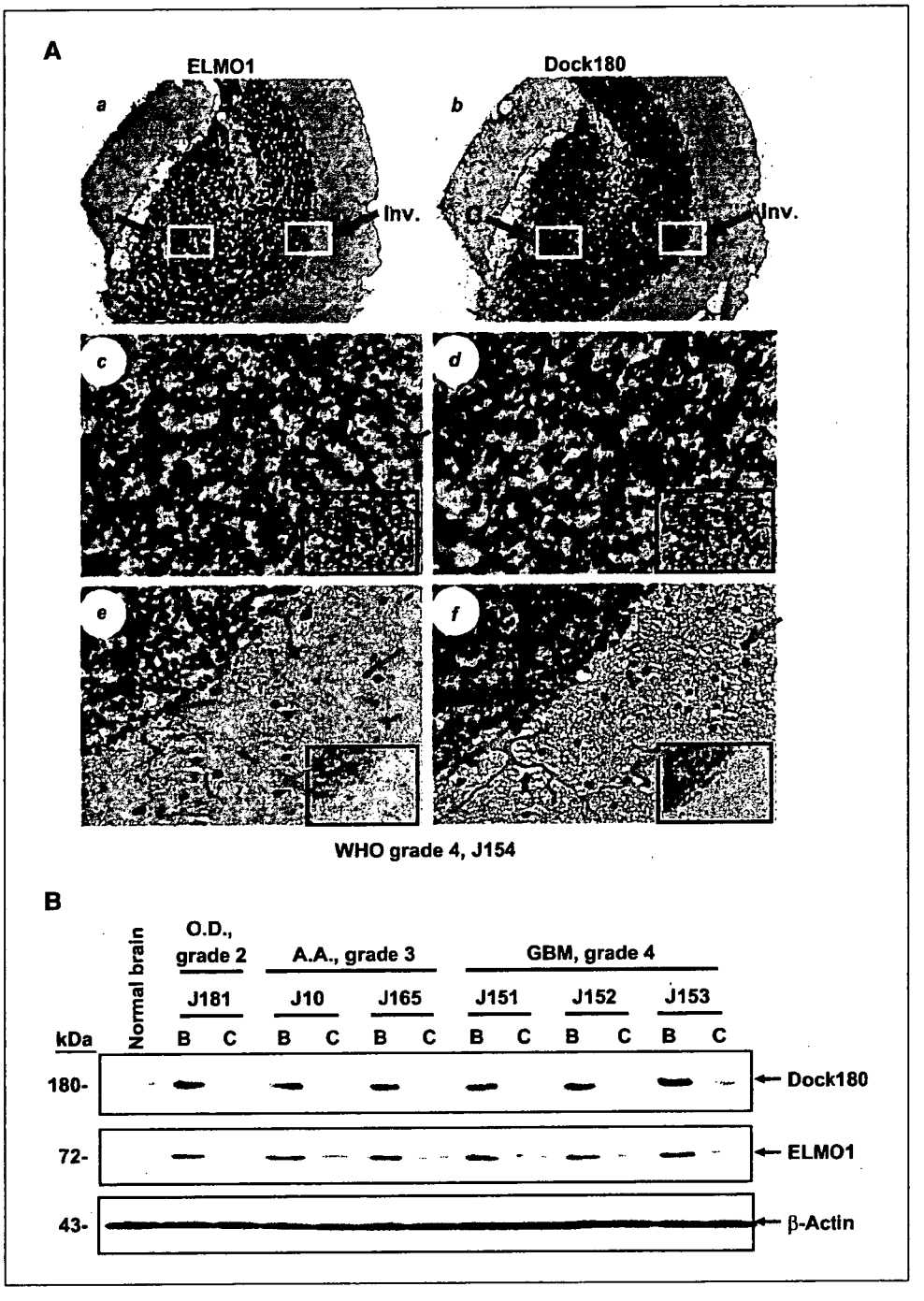

Figure 1. ELMO1 and Dock180 are co-overexpressed in invading tumor cells of primary human glioma specimens. *A*, a total of 53 individual primary tumor specimens (WHO grades 2–4) were analyzed, and representative staining of serial sections of glioblastoma multiforme (specimen J154, grade 4) tissue using a polyclonal rabbit anti-ELMO1 antibody (*a*, *c*, and *e*) and a polyclonal goat anti-Dock180 antibody (*b*, *d*, and *f*) is shown. *c* to *f*, *insets*, isotype-matched immunoglobulin G controls of the identical areas shown. *c* and *d*, enlarged central regions of the tumor mass shown in *a* and *b* (*white rectangle*). *e* and *f*, enlarged invasive areas shown in *a* and *b* (*red rectangle*). *Arrows*, positive staining for ELMO1 (*c* and *e*) and Dock180 (*f*). *Arrowheads*, unstained cells. Original magnification, ×100 (*a* and *b*); 400× (*c–f*). Representative results; immunohistochemical (*IHC*) analyses were done two additional times with similar results. *B*, immunoblot analysis of the tumor center (*C*) and invasive border (*B*) of primary glioma specimens. Total protein extracted from normal brain and microdissected glioma tissue from oligodendroglioma (*O.D.*; specimen J181, grade 2), anaplastic astrocytoma (*A.A.*; specimens J10 and J165, grade 3), and glioblastoma multiforme (*GBM*; specimens J151, J152, and J153, grade 4) was examined by immunoblotting with anti-Dock180 and anti-ELMO1 antibodies, respectively. The membranes were also probed with an anti–β-actin antibody as a loading control. Representative of three independent experiments with similar results.

The ELMO1-Dock180 complex has been shown to stimulate cell migration through the activation of Rac1 (25). Recently, we identified the up-regulation of ELMO1 gene expression in an angiopoietin-2–induced astrocytoma invasion model using global gene array followed by real-time PCR analysis,[8] signifying the potential importance of ELMO1 in promoting glioma invasion. To determine the role of ELMO1 and its binding partner Dock180 (21) in glioma cell invasion, we began by carrying out immunohistochemical analyses on a collection of primary human glioma specimens to assess whether ELMO1 and Dock180 are associated with the invasive phenotype of gliomas. We examined 53 tumors representing WHO grades 2 to 4 containing an identifiable central region and invasive areas and four normal human brain specimens (J140–J143) obtained at autopsy from patients without brain lesions as controls (28). Little to no immunoreactivity for ELMO1 and Dock180 was detected in the normal brain specimens (Supplementary Table S1; Fig. S1, *a* and *b*). Interestingly, the co-overexpression of ELMO1 and Dock180 was found in infiltrating tumor cells within the invasive areas of the glioma specimens independent of tumor grade (Fig. 1*A*, *e* and *f*; Supplementary

[8] Manuscript in preparation.

Table 1. ELMO1 and Dock180 expression correlates with glioma invasion

Immunohistochemical score	ELMO1			Dock180		
	Center	Border	Invasive	Center	Border	Invasive
3+	0	3	9	0	3	10
2+	1	12	19	1	15	22
1+	9	14	7	3	15	15
±	29	15	10	18	16	5
−	14	9	8	31	4	1
P value of correlation between positivity and tumor area*						
Border vs center		<0.01			<0.0001	
Invasive vs center		<0.0001			<0.0001	
Border vs invasive		NS			<0.05	

NOTE: The immunohistochemical staining intensity for each antibody and specimen was defined as no (−), weakest (±), low (1+), medium (2+), and strong (3+) staining as previously described (28) and is shown in Supplementary Table S1. NS, not significant ($P > 0.05$).
*Analyzed by χ^2 test for trend based on the distribution of the scores from each area.

Fig. S1, *e*, *f*, *i*, and *j*). Actively invading glioma cells observed at distant sites such as the gray matter of normal brain parenchyma, along blood vessels, neuronal structures, and the corpus callosum showed a high immunoreactivity for ELMO1 and Dock180 (data not shown). For example, in a glioblastoma multiforme (grade 4) specimen, the glioma cells invading into the adjacent brain structure (Fig. 1*A*, *e* and *f*, *arrows*) exhibited strong immunostaining by the ELMO1 and Dock180 antibodies. In contrast, Dock180 protein was not detected (Fig. 1*A*, *d*) and ELMO1 was expressed at low levels in the central core region of this same glioma tissue (Fig. 1*A*, *c*). Additionally, we failed to detect the expression of ELMO1 and Dock180 in reactive astrocytes or cells that are morphologically similar to astrocytes in invasive areas or center regions in these primary glioma specimens.

To determine whether there is a distinct link between ELMO1 and Dock180 expression and human glioma invasiveness, we did a χ^2 test for trend to examine the association between the positive staining of ELMO1 and Dock180 and each area of the glioma specimen (center, border, and invasive areas). As shown in Table 1, a significant correlation was found between the positive immunoactivities for ELMO1 ($P < 0.01$ for border versus center and $P < 0.0001$ for invasive versus center, respectively) and Dock180 ($P < 0.0001$ for both comparisons) and the invasiveness displayed by these gliomas. Of the 53 glioma samples analyzed, 67% (8 of 12) and 92% (11 of 12) WHO grade 2 specimens, 69% (11 of 16) and 75% (12 of 16) grade 3 specimens, and 84% (21 of 25) and 96% (24 of 25) grade 4 specimens showed higher expression of ELMO1 and Dock180 in the border/invasive areas versus the center region of the tumors, respectively (Supplementary Table S1).

Next, to corroborate our observation of ELMO1 and Dock180 upregulation in invading glioma cells of the primary glioma specimens, we did immunoblotting on total protein extracted from the border/invasive regions and core area of microdissected primary glioma tissues and four normal brain specimens (28) that were used in the immunohistochemical analyses. An increase in ELMO1 and Dock180 expression was found in the border region of all six primary glioma specimens examined when compared with the center tumor area of the identical sample (Fig. 1*B*). Little to no expression of ELMO1 and Dock180 was detected in the normal brain specimens (Fig. 1*B*; Supplementary Fig. S2). These findings

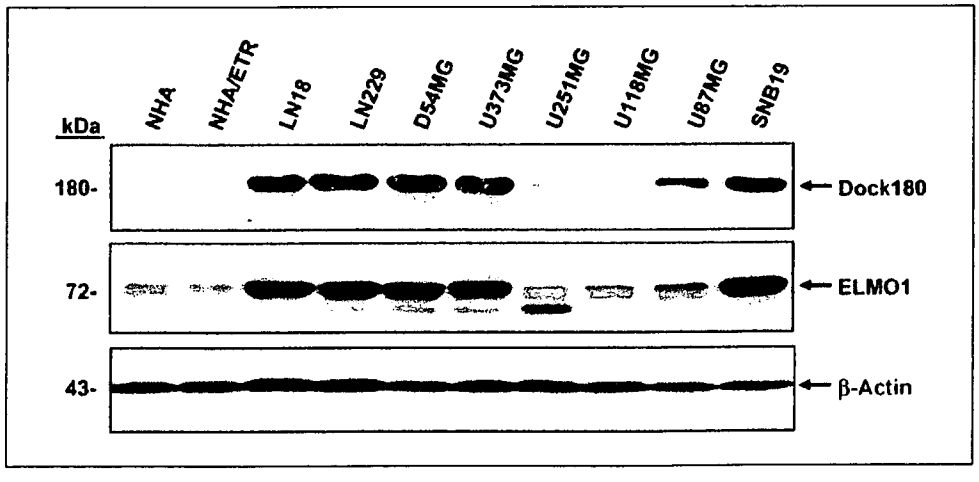

Figure 2. Endogenous expression of Dock180 and ELMO1 in various human glioma cell lines. Immunoblot analysis of normal human astrocytes (*NHA*), genetically modified normal human astrocytes (*NHA/ETR*; see Materials and Methods), and human glioma cell lysates with anti-Dock180 and anti-ELMO1 antibodies. The membranes were also probed with an anti–β-actin antibody as a loading control. Representative of three independent experiments with similar results.

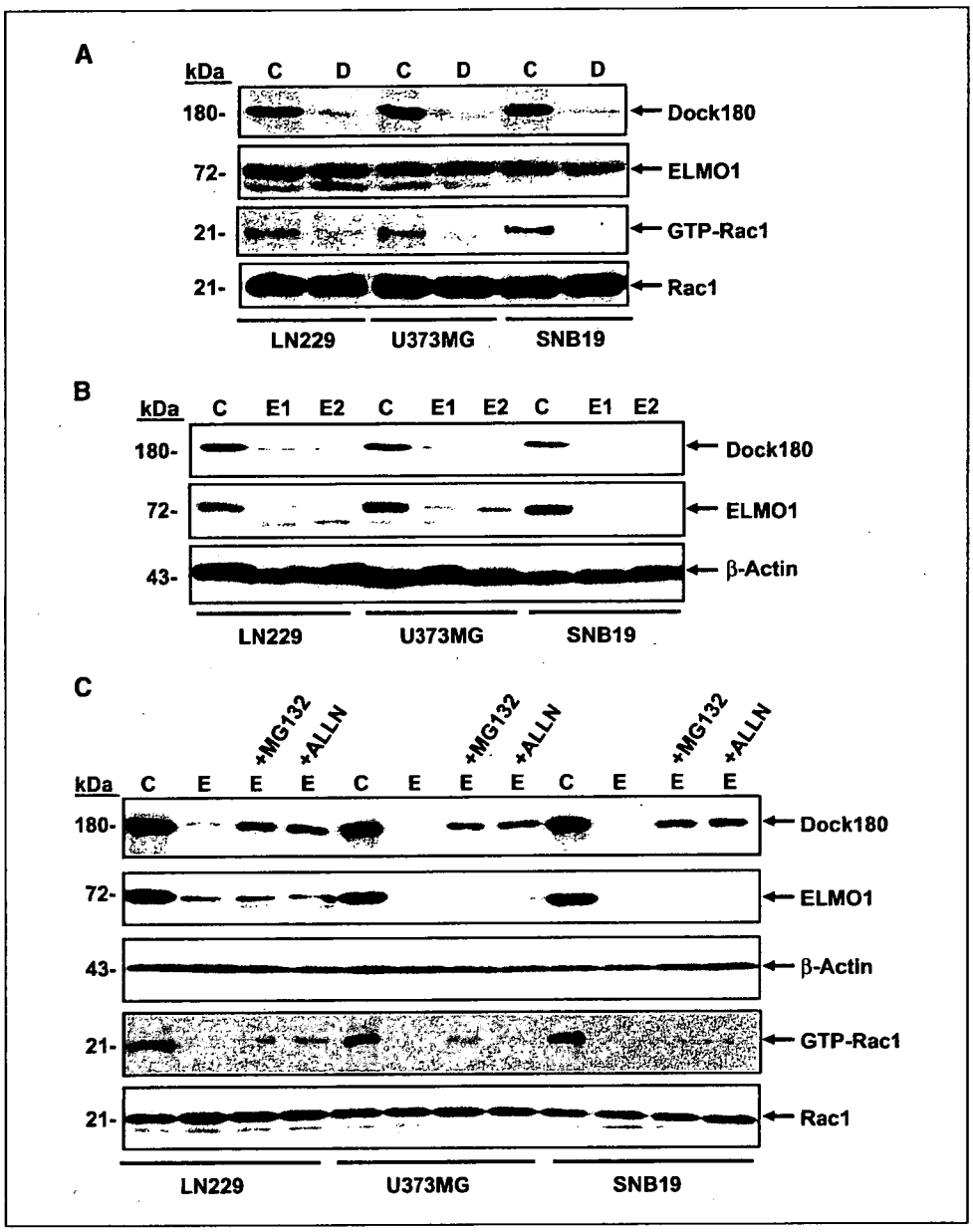

Figure 3. Suppression of endogenous ELMO1 and Dock180 inhibits GTP loading of Rac1 in glioma cells. *A* and *B*, LN229, U373MG, and SNB19 cells were transiently transfected with ELMO1 siRNA (*E1* and *E2*), Dock180 siRNA (*D*), or a control siRNA (*C*). Total cell lysates were analyzed by immunoblotting with anti-ELMO1, anti-Dock180, and anti-Rac1 antibodies and GTP loading of Rac1 using a Rac1 activation assay kit. *C*, LN229, U373MG, and SNB19 cells were transiently transfected with ELMO1 siRNA and treated with the proteasome inhibitors MG132 (2 μmol/L) or ALLN (4 μmol/L) followed by immunoblotting for ELMO1, Dock180, and Rac1 expression and GTP loading of Rac1. The membranes were also probed with an anti–β-actin antibody as a loading control. Representative of three independent experiments with similar results.

support our immunohistochemical data showing that ELMO1 and Dock180 are co-upregulated in the areas of active invasion of primary glioma specimens. Taken together, these data suggest that the expression of ELMO1 and Dock180 is consistent with the intrinsically invasive phenotype of gliomas and independent of tumor grade.

ELMO1 and Dock180 are coexpressed in human glioma cell lines. Next, we sought to determine whether ELMO1 and Dock180 play a role in glioma cell migration and invasion. We first examined the expression of ELMO1 and Dock180 in various human glioma cell lines. As shown in Fig. 2, LN18, LN229, D54MG, U373MG, and SNB19 glioma cell lines endogenously express ELMO1 and Dock180 at high levels whereas lower-level expression was found in normal human astrocytes, genetically modified normal human astrocytes (27), U251MG, U118, and U87MG glioma cell lines. In addition, the level of expression of ELMO1 correlated with the expression level of Dock180.

Inhibition of endogenously expressed ELMO1 and Dock180 suppresses Rac1 activation in glioma cells. ELMO1 and Dock180 have previously been shown to form a complex and act as a bipartite GEF thereby activating Rac1 (21). Therefore, we evaluated the significance of endogenous ELMO1 and Dock180 expression in glioma cells and determined whether inhibition of their expression by siRNA attenuates Rac1 activation. LN229, U373MG, and SNB19 glioma cells were separately transfected with ELMO1 and Dock180 siRNA. After 48 h, the glioma cells that were transiently transfected with a siRNA pool containing three target-specific sequences for Dock180 completely suppressed Dock180 expression and significantly attenuated Rac1 activation while having no effect on ELMO1 and Rac1 protein levels (Fig. 3*A*). Similarly, two different siRNAs for ELMO1 (designated E1 and E2) inhibited ELMO1 expression (Fig. 3*B*), resulting in a decrease in GTP loading of Rac1 without alteration of Rac1 protein expression (Fig. 3*C*). Interestingly, siRNA knockdown of ELMO1 also reduced the expression of Dock180 in

the glioma cells tested (Fig. 3*B* and *C*). This effect was partially blocked by the proteasome inhibitors MG132 and ALLN (Fig. 3*C*), corroborating a previous report showing that ELMO1 protects Dock180 from ubiquitylation-mediated degradation (29). These data suggest that ELMO1 and Dock180 function upstream of Rac1 and play an essential role in its activation in glioma cells.

Suppression of endogenously expressed ELMO1 and Dock180 expression inhibits glioma cell migration and invasion. Rac1, a Rho family GTPase member, induces lamellipodia formation, cell migration, and invasion in glioma cells (6). Therefore, we hypothesize that ELMO1 and Dock180 promote glioma cell migration and invasion through their effects on Rac1 activation. To test this hypothesis, we transiently transfected LN229, U373MG, and SNB19 glioma cells with ELMO1, Dock180, and Rac1 siRNA. As shown in Fig. 4*A* and Supplementary Fig. S3, suppression of ELMO1 and Dock180 expression inhibited *in vitro* glioma cell migration by 3- to 4-fold, comparable to Rac1 knockdown by siRNA (Supplementary Fig. S3). Consistent with these results, knockdown of endogenous ELMO1 and Dock180 inhibited the ability of LN229, U373MG, and SNB19 cells to invade through a growth factor–reduced Matrigel–coated membrane. Again, *in vitro* glioma cell invasion was attenuated to the same degree using ELMO1 or Dock180 siRNA as Rac1 suppression (Fig. 4*B*). These results suggest that ELMO1 and Dock180 have an essential role in promoting glioma cell migration and invasion similar to Rac1.

To test our hypothesis in a pathophysiologically relevant model, we examined whether inhibition of ELMO1 and Dock180 modulates the invasion of SNB19 and U373MG cells in a murine brain slice model (9, 10). We separately transfected GFP-expressing SNB19 and U373MG cells with control, ELMO1, or Dock180 siRNA. After 48 h, the glioma cells that were transfected with specific or control siRNAs were placed bilaterally onto the putamen of a murine brain slice and allowed to invade into the brain tissue for an additional 48 h. Afterwards, lateral migration/invasion and depth of invasion were evaluated. Inhibition of ELMO1 and Dock180 expression in both cell lines displayed less lateral migration/invasion on the brain slice compared with control siRNA–transfected or nontransfected cells (Fig. 4*C* and data not

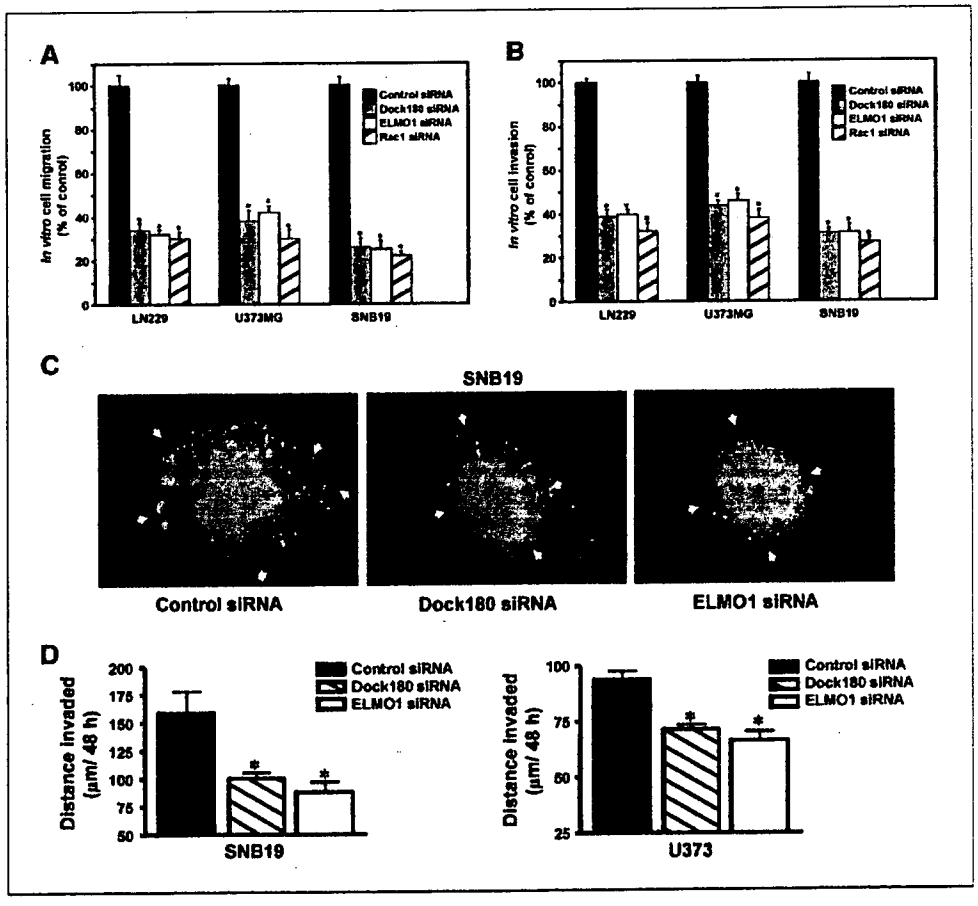

Figure 4. Suppression of endogenous ELMO1 and Dock180 inhibits glioma cell migration and invasion. *A, in vitro* cell migration assay. LN229, U373MG, and SNB19 cells were transiently transfected with the indicated siRNAs followed by cell migration assay. *B, in vitro* cell invasion assay. LN229, U373MG, and SNB19 cells were transiently transfected with the indicated siRNAs followed by an invasion assay. The migrating or invading cells were counted in 10 random high-powered fields (total magnification, ×200). Mean number of migrating or invading control cells: for migration, LN229 cells, 94.2 ± 4.6/field; U373MG cells, 73.1 ± 2.8/field; SNB19, 113.3 ± 3.8/field; and for invasion, LN229 cells, 46.7 ± 1.4/field; U373MG cells, 56.2 ± 1.9/field; SNB19, 37.2 ± 2.4/field. *Columns,* percent of control siRNA cells; *bars,* SD. *, $P < 0.05$, one-way ANOVA followed by Newman-Keuls post hoc. Three independent experiments were done in triplicate with similar results. *C,* GFP-expressing SNB19 and U373MG cells (data not shown) were transiently transfected with indicated siRNAs followed by an *ex vivo* brain slice invasion assay. Representative epifluorescent images of the GFP-expressing SNB19 cells were captured using a digital camera attached to a stereomicroscope at ×40 magnification. *D,* depth of SNB19 and U373MG cell invasion into a murine brain slice. *Columns,* mean distance (μm) invaded in 48 h from six independent experiments done in five to seven replicates per pair (control siRNA–transfected cells versus specific siRNA–transfected cells); *bars,* SE. *, $P < 0.05$, one-way ANOVA followed by Newman-Keuls post hoc. No-transfection controls for both SNB19 and U373MG cell lines were also done showing no observable effects on cell viability or the invasive ability when comparing the control siRNA–transfected and nontransfected cells (data not shown).